Department of Mechanical and
Industrial Engineering
University of Illinois at
Urbana-Champaign
Urbana, IL 61801

UILU-ENG 89-4005

Final Technical Report

EXPERIMENTAL AND NUMERICAL STUDIES OF LASER SUSTAINED GAS PLASMAS

J. Mazumder and H. Krier
Co-Principal Investigators

and

A. Mertogul, S. Schwartz, X. Chen,
J. Eguiguren, and D. Zerkle
Graduate Research Assistants

Final Report Submitted to

Air Force Office of Scientific Research
Dr. Mitat Birkan, Program Manager
for research conducted during the period
1 February 1988 to 15 March 1989
under
Grant No. AFOSR-88-0129

April 1989

FINAL TECHNICAL REPORT

No. UILU-ENG-89-4005

For research supported by
AFOSR Grant No. 88-0129

for period 02/01/88 to 03/15/89

EXPERIMENTAL AND NUMERICAL STUDIES OF LASER SUSTAINED GAS PLASMAS

prepared by

Jyoti Mazumder[1] and Herman Krier[1],
Ayhan Mertogul[2], Scott Schwartz[2], Xiangli Chen[2],
Jose Eguiguren[2], and David K. Zerkle[2]

Department of Mechanical and Industrial Engineering
University of Illinois at Urbana-Champaign
1206 West Green Street
Urbana, IL 61801

Work supported by

Air Force Office of Scientific Research
Dr. Mitat Birkan is Program Manager

(1) Co-Principal Investigators
(2) Graduate Research Assistants

UNCLASSIFIED
SECURITY CLASSIFICATION OF THIS PAGE

REPORT DOCUMENTATION PAGE

1a. REPORT SECURITY CLASSIFICATION: Unclassified	1b. RESTRICTIVE MARKINGS: None
2a. SECURITY CLASSIFICATION AUTHORITY	3. DISTRIBUTION/AVAILABILITY OF REPORT: Approved for public release; distribution is unlimited.
2b. DECLASSIFICATION/DOWNGRADING SCHEDULE	
4. PERFORMING ORGANIZATION REPORT NUMBER(S): UILU-ENG-89-4005	5. MONITORING ORGANIZATION REPORT NUMBER(S): AFOSR-TR- 89-0596
6a. NAME OF PERFORMING ORGANIZATION: University of Illinois at Urbana-Champaign; 6b. OFFICE SYMBOL (If applicable): UIUC	7a. NAME OF MONITORING ORGANIZATION: AFOSR/NA
6c. ADDRESS (City, State and ZIP Code): Dept. of Mechanical & Industrial Engineering, 140 MEB; 1206 W. Green Street; MC-244, Urbana, IL 61801	7b. ADDRESS (City, State and ZIP Code): Building 410, Bolling AFB, D.C. 20332-6448
8a. NAME OF FUNDING/SPONSORING ORGANIZATION: AFOSR/NA; 8b. OFFICE SYMBOL (If applicable): AFOSR	9. PROCUREMENT INSTRUMENT IDENTIFICATION NUMBER: AFOSR Grant No. 88-0129
8c. ADDRESS (City, State and ZIP Code): Building 410, Bolling AFB, D.C. 20332-6448	10. SOURCE OF FUNDING NOS.

PROGRAM ELEMENT NO.	PROJECT NO.	TASK NO.	WORK UNIT NO.
61102F	2308	A1	

11. TITLE (Include Security Classification): Numerical Studies of Laser Sustained Gas Plasmas (U)	
12. PERSONAL AUTHOR(S): J. Mazumder, H. Krier, A. Mertogul, X. Chen, S. Schwartz, J. Eguiguren, D. Zerkle	
13a. TYPE OF REPORT: Final Technical; 13b. TIME COVERED: FROM 2/1/88 TO 3/15/89	14. DATE OF REPORT (Yr., Mo., Day): April 10, 1989; 15. PAGE COUNT: 86
16. SUPPLEMENTARY NOTATION	

17 COSATI CODES			18. SUBJECT TERMS (Continue on reverse if necessary and identify by block number)
FIELD	GROUP	SUB. GR.	Beamed Energy Propulsion; Laser Plasma Formation

19. ABSTRACT

Laser propulsion is the production of high specific impulse rocket thrust using a high power laser as a remote energy source. Specific impulses in excess of 1000 seconds are achievable because propellant temperatures are very high and low molecular weight gases can be used. This report focuses on the energy conversion mechanisms of laser-sustained plasmas in pure flowing argon and argon/helium mixtures. The status of AFOSR sponsored experiments to determine thermal efficiency and global absorption is detailed. In addition the status of the numerical modeling of the fully two-dimensional plasma flowfield is reviewed. -

[OVER SEE REVERSE SIDE]

20. DISTRIBUTION/AVAILABILITY OF ABSTRACT: UNCLASSIFIED/UNLIMITED ☒ SAME AS RPT. ☒ DTIC USERS ☐	21. ABSTRACT SECURITY CLASSIFICATION: UNCLASSIFIED

22a. NAME OF RESPONSIBLE INDIVIDUAL	22b. TELEPHONE NUMBER (Include Area Code)	22c. OFFICE SYMBOL
Dr. Mitat Birkan	(202) 767-4937	AFOSR/NA

DD FORM 1473, 83 APR EDITION OF 1 JAN 73 IS OBSOLETE.

19. Abstract (continued)

Experiments at very high argon mass flux (55 kg/m^{2}s) and pressure as high as 2.5 atmospheres have been performed. The results indicate that nearly all the laser power can be absorbed (>97%), and efficiencies approaching 50% can be obtained. Experiments with mixtures of argon and helium indicate that the high specific heat and thermal conductivity of the helium tends to allow for more of the absorbed energy to be retained rather than reradiated to the chamber walls. This despite the fact that the very high ionization energy of helium limits the global absorption to values below that for pure argon plasmas. The results show promise for future experiments with hydrogen plasmas.

Fundamental research concerning laser sustained plasmas such as the independent experimental determinations of electron number density and electron temperature is required. This will allow the evaluation of the local thermal equilibrium which is needed in order to better interpret the spectroscopic and numerical results. Also required is the more accurate determination of downstream plasma exhaust gas temperature via Rayleigh scattering thermometry. This technique is impervious to plasma and laser irradiation interferences and to gas heat loss to the chamber walls, thus thermal efficiency calculations will be much more accurate than in the past.

Research into the area of enhanced thermal mixing of the extremely high temperature gas with forced cold convection is called for. Further multiple plasma testing also is required, as are the continued testing of low molecular weight gas plasmas and the numerical study of gas plasmas.

Abstract

Laser propulsion is the production of high specific impulse rocket thrust using a high power laser as a remote energy source. Specific impulses in excess of 1000 seconds are achievable because propellant temperatures are very high and low molecular weight gases can be used. This report focuses on the energy conversion mechanisms of laser-sustained plasmas in pure flowing argon and argon/helium mixtures. The status of AFOSR sponsored experiments to determine thermal efficiency and global absorption is detailed. In addition the status of the numerical modeling of the fully two-dimensional plasma flowfield is reviewed.

Experiments at very high argon mass flux (55 kg/m^2s) and pressure as high as 2.5 atmospheres have been performed. The results indicate that nearly all the laser power can be absorbed (>97%), and efficiencies approaching 50% can be obtained. Experiments with mixtures of argon and helium indicate that the high specific heat and thermal conductivity of the helium tends to allow for more of the absorbed energy to be retained rather than reradiated to the chamber walls. This despite the fact that the very high ionization energy of helium limits the global absorption to values below that for pure argon plasmas. The results show promise for future experiments with hydrogen plasmas.

Fundamental research concerning laser sustained plasmas such as the independent experimental determinations of electron number density and electron temperature is required. This will allow the evaluation of the local thermal equilibrium which is needed in order to better interpret the spectroscopic and numerical results. Also required is the more accurate determination of downstream plasma exhaust gas temperature via Rayleigh scattering thermometry. This technique is impervious to plasma and laser irradiation interferences and to gas heat loss to the chamber walls, thus thermal efficiency calculations will be much more accurate than in the past.

Research into the area of enhanced thermal mixing of the extremely high temperature gas with forced cold convection is called for. Further multiple plasma testing also is required, as are the continued testing of low molecular weight gas plasmas and the numerical study of gas plasmas.

Table of Contents

Chapter 1. Laser Rocket Propulsion

1.1. Introduction

The development of lasers in the megawatt power range coupled with new more durable laser optics will make laser rocket thrusters an extremely promising technology for use in orbital transfer vehicles (OTV's). The laser thruster will operate by collecting and focusing a high power laser beam into an absorption chamber onboard a lightweight OTV. Here the laser energy is absorbed by a low molecular weight gas plasma sustained near the focus of the laser beam. The gas thus heated by the laser sustained plasma (LSP) is then expanded out a converging-diverging nozzle to produce thrust.

Using 10 megawatts of laser power, thrusters will be capable of producing specific impulses greater than 1000 seconds with moderate thrust levels (greater than 1 kN) [1]. Specific impulse is the figure of merit for efficiency of rocket propulsion systems. It has units of seconds and is defined as the thrust produced divided by the weight (at sea level) of propellant expelled per second. Since the payload mass fraction of an OTV (or any spacecraft) depends on the specific impulse, a high specific impulse is very desirable.

The specific impulse depends on propellant stagnation temperature and molecular weight as shown below where I_{sp} is the specific impulse, T_o is the propellant stagnation temperature and MW is the propellant molecular weight.

$$I_{sp} \sim \sqrt{\frac{T_o}{MW}} \tag{1.1}$$

The stagnation temperature depends on the absorption chamber wall temperature limit and the amount of power absorbed, which is a function of the input laser power. The molecular weight of the propellant gas depends solely on the choice of propellant gas. Therefore by using a low molecular weight propellant (such as hydrogen) with high laser powers, a high specific impulse can be achieved.

The relationship between thrust, specific impulse, and input laser power in a laser thruster can easily be derived as follows. The thrust is equal to the mass flow rate times the propellant exhaust velocity. Using the definition of specific impulse it follows that

$$F = \dot{m}\, I_{sp}\, g_o \tag{1.2}$$

where F is the thrust, $\dot{m}$ is the mass flow rate and g_o is the gravitational constant.

Defining thermal efficiency as the fraction of input laser power retained as thermal energy by the flowing propellant (and converted to kinetic energy in the exhaust nozzle assuming a nozzle efficiency of one), we have:

$$\eta = \frac{(\frac{1}{2})\, \dot{m}\, C^2}{P_{input}} \tag{1.3}$$

where C is the propellant exhaust velocity and P_{input} is the input laser power.

Eliminating mass flow rate from (1.2) and (1.3) yields the relation between thrust and specific impulse:

$$F = \frac{2\, \eta\, P_{input}}{g_o\, I_{sp}} \tag{1.4}$$

Thus specific impulse is inversely proportional to thrust in a laser thruster for a fixed value of thermal efficiency [2]. Thrust will increase with input laser power despite the specific impulse in the denominator of (1.4) which will also increase with input laser power. This is because the thrust dependence on input laser power as given in (1.4) is greater than the specific impulse dependence on input laser power which was discussed previously.

Expected laser thruster performance fills an existing performance gap between electric propulsion systems and chemical propulsion systems. Electric systems typically have a high specific impulse but a low thrust. These systems are thrust limited due to limitations on the available input power. The power source in an electric rocket, whether it is a nuclear reactor, a grid of solar collectors or simply batteries is heavy and usually inefficient [3]. Chemical

propulsion systems typically have a high thrust but a low specific impulse and are thus specific impulse limited. The same two factors that allow laser thrusters to have a high specific impulse restrict the specific impulse of a chemical rocket. The propellant stagnation temperature is limited by the heat of reaction of the chemical fuel and is typically 2800 to 4400 K. The molecular weight of the propellant gas is not a choice as in a laser thruster but is determined by the reactants used and is typically 9 to 29 kg/kg-mole [3]. For a further discussion of laser propulsion techniques and projected advantages see References 4 and 5.

1.2. LSP Energy Conversion

1.2.1. LSP Absorption

A laser beam with a power density less than 10^9 Watts/cm^2 will pass through cold argon gas without being absorbed [6]. Thus extremely high power density is required to initially ionize (breakdown) a cold gas. Once the gas has been ionized and a LSP is formed, the power density required to sustain it is significantly less than for breakdown, and depends on mass flux through the plasma and beam focusing geometry.

Since the 10 kW laser used in this work cannot generate power densities high enough to ionize cold argon even when the beam is focused by our optics to a spot of ~1 mm, an alternate initiation method is used. The laser beam is brought to a focus on the surface of a tungsten rod. The tungsten rod releases free electrons via thermionic emission and laser heating. Once the free electrons are present, absorption can begin and a LSP is initiated. The tungsten target remains in the beam for only a fraction of a second and is then removed. This technique of initiation requires a laser power density of only 10^5 Watts/cm^2 [6].

The dominant mechanism by which laser radiation is absorbed by the plasma is referred to as inverse bremsstrahlung (IB) absorption. In this process free electrons in the presence of atoms or ions absorb laser photons and gain kinetic energy. Through collisional processes with the heavy particles the entire gas becomes heated. For a more complete description of gas breakdown and stable plasma formation conditions see Ref. 6.

The absorption coefficient of the LSP increases with the number of free electrons available for IB absorption (as would be expected) and this electron number density is directly related to gas pressure. The temperature dependence of the absorption coefficient shows a peak near 16,000 K at one atmosphere pressure. References 7 and 8 contain information on plasma absorption coefficients. The variation of absorption coefficient with temperature and pressure is key to understanding energy conversion trends as will be seen in Chapter Five.

1.2.2. LSP Losses

Simply stated, a LSP is stable if the total plasma losses do not exceed the absorbed power. The key LSP loss mechanisms are radiation, convection and conduction to the surroundings, the latter two being desirable since they serve to heat the propellant gas. Radiation from the plasma can be reabsorbed by the plasma or transmitted to the absorption chamber walls. Although regenerative techniques may be used to recover most of the transmitted energy, the purpose of this work is to study LSP energy conversion trends without the influence of outside aids such as regeneration. Therefore this transmitted radiation is considered lost for our purposes and must be minimized for maximum heat transfer to the propellant gas.

The key figures of merit in this work are the global absorption and thermal efficiency. Global absorption is defined as the percentage of input laser power that is absorbed by the LSP. Thermal efficiency is defined as the percentage of input laser power that is retained by the propellant gas. Because much of the absorbed power is reradiated by the LSP and consequently lost, the global absorption is always found to be higher than the thermal efficiency.

The plasma radiation consists of line radiation and a continuum radiation components. The line radiation is due to downward electron transitions between bound states in atoms (bound-bound transitions). The continuum radiation is due to both recombination of electrons and ions (free-bound transitions) and bremsstrahlung radiation from free electrons in the presence of a heavy particle (free-free transition).

As with the plasma absorption coefficient, plasma radiation behavior with respect to temperature and pressure is key in understanding energy conversion trends. Continuum radiation and line radiation in argon have been studied by Oettinger [9] and Kozlov [10] respectively, and both have been found to be functions of temperature and pressure. No emission peak is seen with respect to temperature, and an increase in pressure is known to increase total radiation loss [1].

1.3. LSP Equilibrium Position

A LSP will exist in an equilibrium state when input power density exactly balances losses due to radiation, conduction and convection. Gas upstream of the plasma is heated by conduction and plasma radiation at a rate determined by the laser input power density and gas velocity. For a given input power density and gas pressure, a LSP will have a plasma wave velocity such that the LSP will remain stationary only if this velocity matches the input gas velocity as shown in Figure 1.1. If the gas velocity is too low, the LSP will propagate in an upstream direction and if the gas velocity is too high, the LSP will propagate downstream or become unstable (meaning that total losses have exceeded power input and the LSP has blown out). For a parallel laser beam this means that the slightest variation in gas velocity or laser power could cause the LSP to shift position drastically or become unstable. In an actual system this marginal stability would be very undesirable. This problem is easily dealt with by focusing the laser beam to a small spot. A focused laser beam would not only produce a more position stable plasma but would also allow for a higher power density than a parallel beam. There is a further examination of LSP stability in a focused beam in Ref. 1.

1.4. Literature Review

LSP's with application to rocket propulsion were first studied in 1974 by Fowler [11] using a 15 kW continuous CO_2 laser in non-forced air. The LSP's were initiated using an electric arc to provide free electrons at the laser focus. Fowler found that LSP's with an f-number (ratio of the focusing optics focal length to the beam diameter) less than ten were stable. Fowler suggested the reason for this f-number limit was that at higher f-numbers the

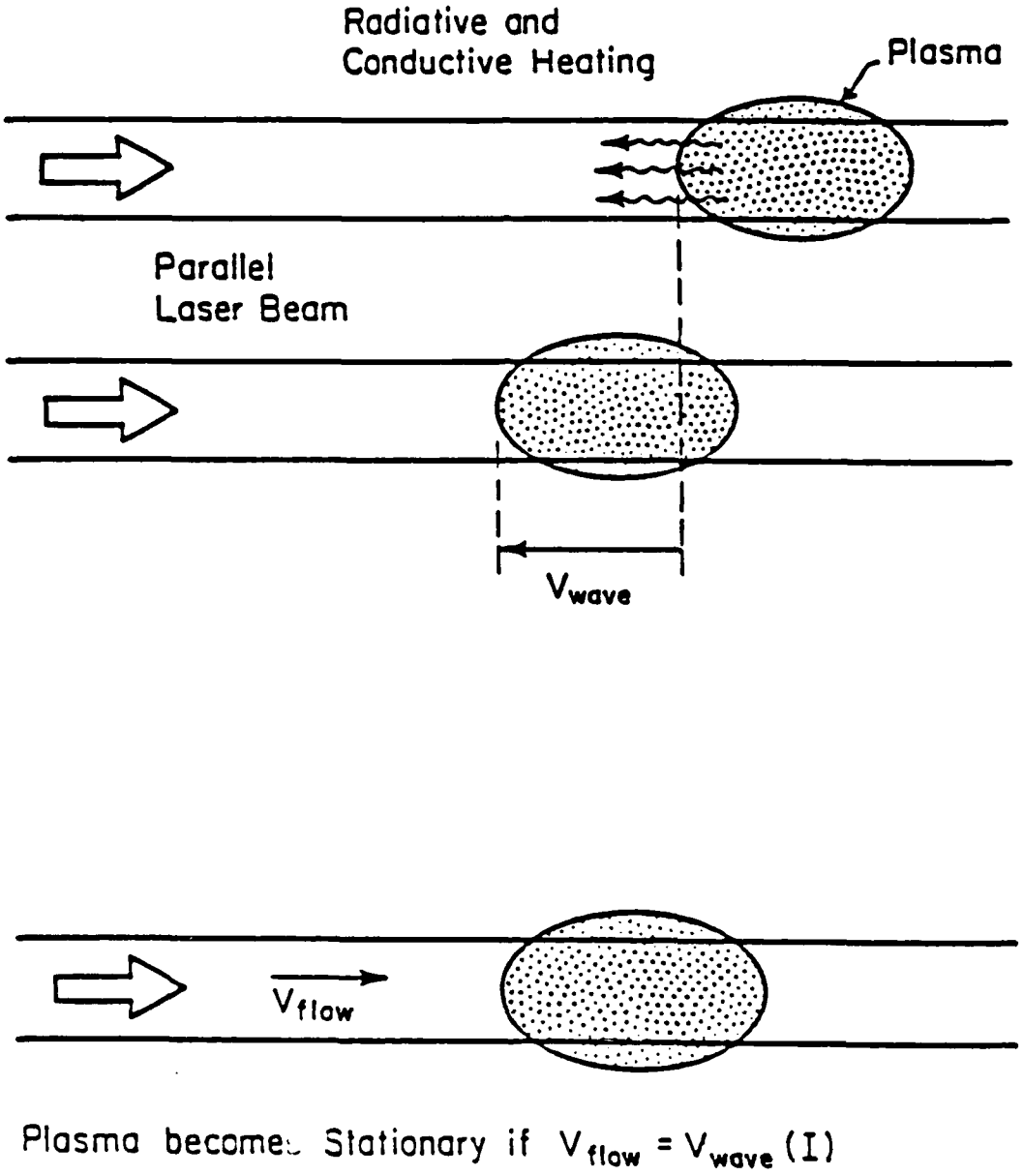

Figure 1.1 A LSP in a parallel beam will move up the beam at a velocity (V_{wave}) that is a function of the input laser power density and gas pressure. The LSP can be stabilized by injecting a flow of gas at a velocity (V_{flow}) exactly equal to the wave velocity. Taken from Ref. 1.

LSP could not respond quickly enough to slight perturbations. An interferometric technique was utilized to obtain electron number density in the plasma, and a plasma temperature distribution was calculated (under the assumption of local thermodynamic equilibrium), resulting in a peak temperature of 15,000 K. Global absorption was found to be as high as 50%, and to rise with laser power. Plasma radiation was cited as the most important energy loss mechanism.

Van Zandt at NASA-Marshall conducted experiments in flowing hydrogen to study hydrogen LSP's and map plasma core temperatures using absolute continuum radiation from the LSP [12]. The LSP's were initiated using a 6 joule 100 nanosecond pulsed CO_2 laser and were sustained by a 30 kW CW CO_2 laser, both focused through the same optics. The output from a filtered video camera was computer analyzed to get an absolute intensity profile of the continuum radiation of the plasma from which an electron temperature distribution was calculated.

Keefer and co-workers at the University of Tennessee Space Institute (UTSI) have conducted experiments in flowing argon to study the effect of varying f-number, flow velocity, and pressure on argon LSP's [13,14]. Pressures up to 4 atmospheres and flow velocities up to 4.5 m/s were studied using a sub-kilowatt CW CO_2 laser. Global absorption as high as 83% and thermal efficiency as high as 38% were reported. In addition, plasma core temperatures over 15,000 K were mapped using a system similar to Van Zandt's based on the absolute continuum radiation of argon at 626.5 nanometers. Keefer showed that high gas flow velocities could be used to force the LSP downstream towards the focus which results in higher global absorption and thermal efficiency [13].

Recently Keefer and Jeng used a new CO_2 laser with a Gaussian beam profile to conduct experiments in flowing argon [15]. Global absorption with the Gaussian beam was found to be less than that for the old annular beam, but the thermal efficiency using the Gaussian beam was higher. A numerical calculation also found that plasmas sustained with shorter wavelength lasers were longer in axial extent, and that they had a lower global absorption.

Krier, Mazumder and graduate students at the University of Illinois at Urbana-Champaign (UIUC) began studying forced argon LSP's in 1983 using a 10 kW CW CO_2 laser. As mentioned previously the LSP's were initiated using a tungsten rod momentarily inserted into the beam focus to provide free electrons. The effects of input laser power, focusing f-number, pressure, and mass flux on global absorption and thermal efficiency have been studied using two independent diagnostic techniques. Calorimetry is used to measure global absorption and thermocouple measurements are used to determine thermal efficiency. In addition a relative line to continuum spectroscopic technique using an Optical Multichannel Analyzer (OMA) system is used to measure plasma core temperatures which have been found to be as high as 20,000 K. Plasma core temperatures can then be used along with the beam geometry to determine global absorption and thermal efficiency [16]. Global absorption measurements agree well for the two techniques but there is a definite discrepancy in the thermal efficiencies. It is believed that the spatial coarseness of the spectroscopic method is the major source of this discrepancy. Early results indicated global absorptions approaching 80% and thermal efficiencies as high as 25% [17].

To supplement and guide the experimental research a quasi two dimensional model was developed [18] which predicted global absorption and thermal efficiency for a wide range of operating conditions in flowing argon. Currently this code is being made fully two dimensional and is being modified to run for hydrogen. A complete listing of work done at UIUC since 1983 appears in Table 1.1.

The results to be discussed in this work were presented in the paper by Zerkle, et al. which appears as entry number ten in Table 1.1 and was presented at the 20th AIAA Thermophysics, Plasmadynamics and Lasers Conference [19]. These latest results include a global absorption as high as 97% and a thermal efficiency as high as 46%.

Table 1.1 Summary of work done on LSP's at UIUC since 1983

Lead Author	Title	Year	Reference
1. R. J. Glumb	Concepts and Status of Laser Supported Rocket Propulsion	1984	4
2. T. D. Bender	Engineering Design, Fabrication, and Performance Evaluation of Laser Heated Gas Flow Facility : Application to Laser Propulsion (M.S. Thesis)	1985	20
3. R. J. Glumb	Experimental and Theoretical Studies of Laser-Sustained Argon Plasmas for Application to Laser-Supported Rocket Propulsion (Ph.D. Thesis)	1986	1
4. R. J. Glumb	A Two-Dimensional Model of Laser-Sustained Plasmas in Axisymmetric Flow Fields	1986	18
5. H. Krier, et al.	Studies of CW Laser Gas Heating by Sustained Plasmas in Flowing Argon	1986	17
6. T. J. Rockstroh	The Role of the Plasma During Laser-Gas and Laser-Metal Interactions	1987	6
7. B. K. McMillin	Energy Conversion in Laser Sustained Argon Plasmas for Application to Rocket Propulsion (M.S. Thesis)	1987	21
8. J. Mazumder, et al.	Spectroscopic Studies of Plasmas During CW Laser Heating in Flowing Argon	1987	16
9. D. K. Zerkle	Energy Conversion Measurements in Laser-Sustained Argon Plasmas at Elevated Mass Flux and Pressure (M.S. Thesis)	1988	22
10. D. K. Zerkle, et al.	Laser-Sustained Argon Plasmas For Thermal Rocket Propulsion	1988	19
11. X. Chen	Spectroscopic Diagnostics of Argon Plasmas During Laser-Gas Interaction (M.S. Thesis)	1988	23
12. A. E. Mertogul	Energy Absorption and Thermal Conversion Efficiency in Argon Laser Sustained Plasmas (M.S. Thesis)	1988	24

1.5 Research Objectives

The main objectives of this investigation continue to be the characterization of laser sustained plasmas and the determination of performance trends useful for laser thruster design. The characterization of LSP's includes the study of fundamental plasma physics. The interaction of the laser with the plasma constituents and the resulting energy transfer is an important issue concerning LSP behavior. The most recent experiments have focused on the optimization of the key performance parameters, global absorption and thermal efficiency.

Although argon gas has been the working gas in all experiments to date, there is a need to extend the investigation to hydrogen gas. Experiments involving helium/argon mixtures have spurred this interest and plans will be discussed for the implementation of a system suitable for working with hydrogen.

The accurate numerical modeling of LSP's is a key element to scaling plasma performance trends to the conditions which might exist in a full-scale thruster. Thus a two-dimensional model is currently being implemented with argon as the working gas in order to draw comparisons with the experimental results. The model can easily be extended to hydrogen for the purposes of guiding such experiments and making full-scale extensions of the operating conditions.

There is also a need for highly precise, adiabatic measurements of thermal efficiency. The current temperature measurements are subject to some certain but as yet undetermined error due to heat loss from the plasma exhaust gas. A method will be described by which highly accurate temperature determinations can be made immediately downstream from a plasma. This is important for the calculation of highly reliable thermal efficiency to be compared with both numerical calculations and independent spectroscopic diagnostics of plasma performance.

Chapter 2. Plasma Physics

Understanding the physics of laser sustained plasmas is important for the application of LSP's to any technology, including laser rocket propulsion. The interaction of an intense laser radiation field with the constituent electrons, ions, and neutral particles of a plasma determines the energy absorption behavior of the plasma and affects the thermodynamics of the plasma system. Radiation losses from the plasma then determine the net amount of incident laser energy that is retained by the plasma as thermal energy. In addition, the rate at which gas flows through the plasma system affects the thermodynamics and overall plasma performance (i.e. absorption and thermal conversion efficiency).

The physics of plasmas at the experimental conditions obtainable in the laboratory must be fully understood in order to make valid extrapolations for the performance of plasmas sustained by much higher power lasers. These extrapolations in conjunction with computer modeling form the basis for assessing the feasibility of LSP based rocket systems.

Local thermodynamic equilibrium (LTE) assures that a single temperature can be defined which applies to the plasma system at any point. This temperature may vary from point to point, but at each point thermal equilibrium exists. This means that the electron kinetic temperature, excited state temperature, and ion temperature are all the same at a point in the plasma. Another way of stating this is that the Maxwellian distributions of electron and heavy particle velocities are governed by the same temperature, and that this temperature satisfies the Boltzmann distribution of excited state populations and the Saha ionization equation [25].

The requirement of LTE in a LSP is of utmost importance to spectroscopic and numerical studies. For instance, the relative line to continuum spectroscopic technique used in this investigation results in the calculation of temperature. Under LTE this temperature can be used to determine the plasma composition (in terms of electron number density, neutral particle number density, etc.), the local absorption coefficient in the beam path, and the emissive power at every point in the plasma. The absorption and emission are defined in terms of electron temperature, and thus if the temperature measured spectroscopically is not a good estimate of

this temperature (as would be the case if the plasma were not in LTE) then the technique cannot reliably be used.

Similarly, in the numerical work of this investigation a single temperature governs all the energy transfer processes being modelled, and thus it is strictly valid only in cases of LTE. In addition all gas property and composition data is based on LTE calculations [26]. The inclusion of non equilibrium (two particle temperatures) effects into a numerical routine is possible, but will not be pursued until a more complete understanding of plasma equilibration processes is had.

The topic of LTE validity is not new to laser sustained plasma research. In the past, LSP's have been assumed to be in LTE based on their high density at one atmosphere pressure and above [1,6,12,13,14,16,18]. The argument is that the rate of collisional excitation and de-excitation processes within an atom dominates the radiation rates. This implies an electron number density on the order of 10^{17} cm^{-3}. In addition, the laser energy absorption is heavily dominated by electrons, and it is assumed that the electron-heavy particle collisions are frequent enough to overcome the tremendous mass ratio and equilibrate the plasma temperature. It is not at all clear, however, that true LTE exists in LSP's at all pressures, especially in regions of high beam irradiance in which the electrons gain so much energy in such a short period of time that the electron temperature is probably quite higher than the heavy particle temperature [27].

A focused high power laser beam has associated with it a very strong electric field. If the energy taken by an electron from this field over its mean free path is larger than the energy it can transfer in a heavy particle collision, then the electron and heavy particle temperatures will not be equal [27]. The electric field strength criterion is as follows [27],

$$E^2 << (5.5 \times 10^{-12} N_e \frac{E_H}{kT})^2 \frac{m}{M} \qquad (2.1)$$

where E is the electric field strength in Volts/meter, N_e is the electron number density in cm^{-3}, E_H is the ionization energy of hydrogen, m is the electron mass, and M is the mass of the heavy particles.

If equilibrium values are taken for T and N_e, this inequality is not satisfied for argon plasmas at one atmosphere and 20,000 K under the irradiation of 3×10^9 W/m^2 (corresponding to 2.5 kW focused to a 1 mm spot). The electric field strength is 1.5×10^6 V/m at this irradiance, while the right hand side of the above equation is only 8.3×10^8.

It seems that the plasma regions directly affected by the laser beam are not in LTE, but that there may be regions in the plasma periphery and downstream of the focus point that are in LTE. Another possibility is that the plasma can be in partial LTE, that is, the electron temperature accurately describes the extent of ionization and the population of excited atomic states, but not the distribution of heavy particle kinetic energies.

The line-to-continuum spectroscopic technique will return a meaningful temperature measurement only when the excited states of the plasma atoms are in equilibrium with the free electrons. The line emission intensity, in general, is a function of the population distribution of excited atomic states. The continuum emission has two components, one is bremsstrahlung radiation which is a function of free electron temperature, and the other is recombination radiation which is a function of both free electron temperature and the excited state populations.

In order to place greater confidence in the results of this normally accurate (under LTE) spectroscopic technique it will be necessary to make independent measurements of the electron number density. The logic behind this is that electron number density has been calculated as a function of temperature for plasmas in LTE [26]. If these calculations give a temperature corresponding to the measured electron number density that is the same as the temperature resulting from the line-to-continuum ratio, then it is quite likely that the excited state populations, extent of ionization, and electron energy distribution can all be described by the same temperature.

If the results of the LTE calculations do not agree with the line-to-continuum results, then the absorption and emission coefficients which are calculated under the LTE assumption cannot be confidently applied in calculating global absorption and thermal conversion efficiency of the LSP's.

From the standpoint of the numerical calculations not only are the absorption and emission coefficients critical, but so is the kinetic temperature of the heavy particles. This is because most thermophysical properties of plasmas depend partly upon the kinetic energy of the constituent heavy particles. If the current models are to be relied upon to provide accurate extrapolations to operating conditions not available in the laboratory, then the plasma must be in LTE as applied to the heavy particle kinetic temperatures as well.

It is anticipated that measurements of the heavy particle temperature can be made directly [27]. Again, we hope that the results of the measurements will agree with the line-to-continuum spectroscopic technique. But in the event that there is significant discrepancies, then it may be necessary to explore multi-temperature non-equilibrium modelling of plasmas.

The equilibrium status of laser sustained plasmas must be defined if model verification and extrapolation to practical operating conditions is to be realized. This may be accomplished through experimental measurements of electron number density and temperature [28], and possibly the heavy particle temperature in the plasma.

The electron number density can be calculated from the Stark broadened linewidth of plasma emission [27]. Stark broadening results from the presence of charged particles in the plasma and is well documented for certain lines of hydrogen emission [29]. Thus if small amounts of hydrogen of seeded into an argon plasma, or if a hydrogen plasma is being examined, the electron number density can be determined. From this and from measured population densities of a number of excited states, the electron temperature can be deduced [28].

The most well established method for determining heavy particle kinetic temperature is to determine the Doppler broadened linewidth of plasma emission. This linewidth is directly related to the Doppler shift associated with particles in thermal motion and can therefore be used to determine the kinetic temperature of heavy particles. The problem is that at high pressure (certainly at one atmosphere) the Doppler broadening is overwhelmed by pressure broadening mechanisms such as Stark broadening and cannot be accurately resolved.

There is hope, however, that laser light scattered from the plasma constituents may give information concerning the density of the heavy particles, and by applying an appropriate equation of state, the temperature may be determined. This is an area that will require a great deal of attention and very detailed experimentation and data reduction. The presence of very high temperatures and scattering from the free electrons may prove to be the undoing of such an experiment.

The conditions downstream of the plasma do not present nearly so challenging a measurement environment and the Rayleigh scattering of ultraviolet laser light from the lower temperature neutral particles in this region can be used to determine temperature [30]. Rayleigh scattering is an elastic process for which the wavelength of scattered radiation is the same as the wavelength of the incident radiation. Therefore instantaneous two dimensional mappings of the downstream temperature field will be possible because wavelength resolution can be accomplished with an interference filter rather than a spectrograph/monochromator. The latter method restricts measurements to a single spatial dimension because the spectral components are spread across the other dimension.

Measurements of Rayleigh scattered radiation will be the basis for the high accuracy efficiency calculations mentioned above. Rayleigh scattering intensity is proportional to heavy particle density and can therefore be used to gauge temperature. Rayleigh scattering thermometry downstream of the plasma region is unaffected by the plasma equilibrium status and can be confidently used as a check for both numerical and spectroscopic results. The apparatus and procedures for this technique will be outlined in Chapter 6.

As in all LSP research thought must be given to the ramifications of using hydrogen rather than argon as the working gas, and the possibility that full-scale laser thrusters may be operated at elevated pressures. The discussions presented here concerning LTE apply to all gases, and hydrogen also fails to satisfy equation 2.1 at atmospheric pressure. It would seem a worthy goal to explore the equilibrium status of the laboratory plasmas at elevated pressure as well in an effort to better understand the physics of laser sustained plasmas.

Chapter 3. Experimental Facility

3.1. Laser and Optics

A schematic representation of the laser facility is shown in Figure 3.1. Safety switches on the laser control room and diagnostics room doors as well as the outside door to the lab prevent the laser from operating if any of the doors are open. The laser beam propagates horizontally across the lab approximately a meter and a half above the floor to the test stand shown schematically in Figure 3.2. Two different focal length lenses were used in this work, a 21 inch focal length NaCl lens and a new 12 inch focal length zinc selenide (ZnSe) lens. These focal lengths correspond to f-numbers of approximately 7.1 and 4.1 respectively. Zinc selenide is an extremely durable material which when anti-reflective coated is over 99% transmissive to 10.6 μm radiation and which has many advantages over NaCl. One such advantage of ZnSe is that it can be exposed to water and cleaned with acetone. Therefore the lens surfaces can be kept cleaner than NaCl resulting in less power absorption by the lens and less thermal stress within the lens. The ZnSe laser inlet window is mounted to the bottom of the absorption chamber above the lens. Watercooled ZnSe was used in place of NaCl because ZnSe has twice the rupture modulus of NaCl and a linear expansion coefficient with respect to temperature (dL/dT) less than a fifth that of NaCl [31]. A further discussion of the steering and focusing optics can be found in References 19, 22.and 24.

Losses in the optics are based on laser power calibrations performed in front of the test stand and after the beam has passed through the optics. Optical losses vary almost linearly with laser input power between approximately 9% at 2.5 kW laser input power and approximately 27% at 10 kW laser input power (using a ZnSe window and the 12 inch focal length ZnSe lens). Losses are due to power absorption by the mirrors, and absorption and reflection by the lens and window. Losses vary slightly depending on the type of lens and window material with the ZnSe components having less losses than the NaCl components as mentioned previously. Although the laser is capable of outputting 10 kW, this 27% loss limits

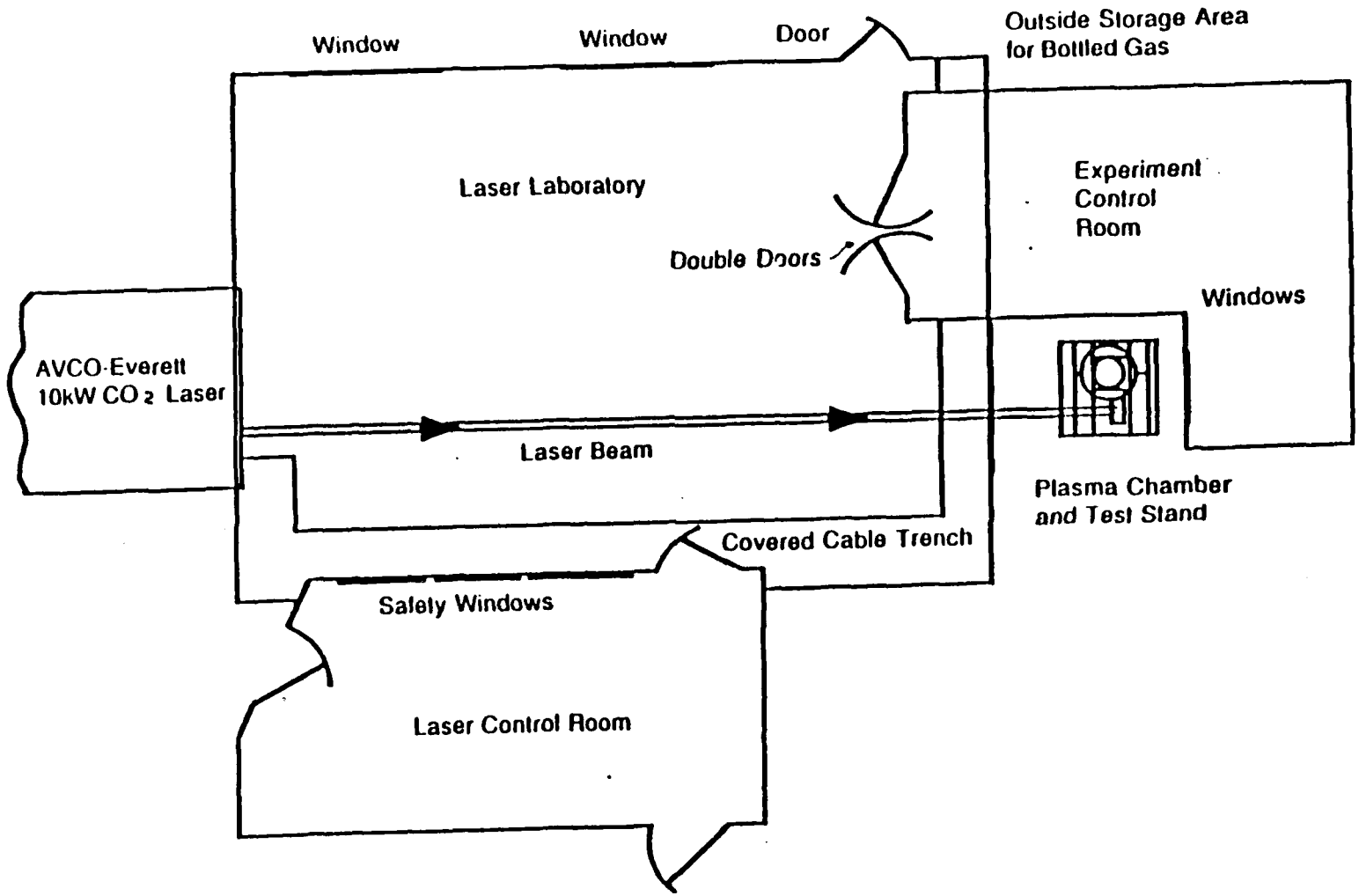

Figure 3.1 Schematic of the experimental laser facility. Taken from Reference 21.

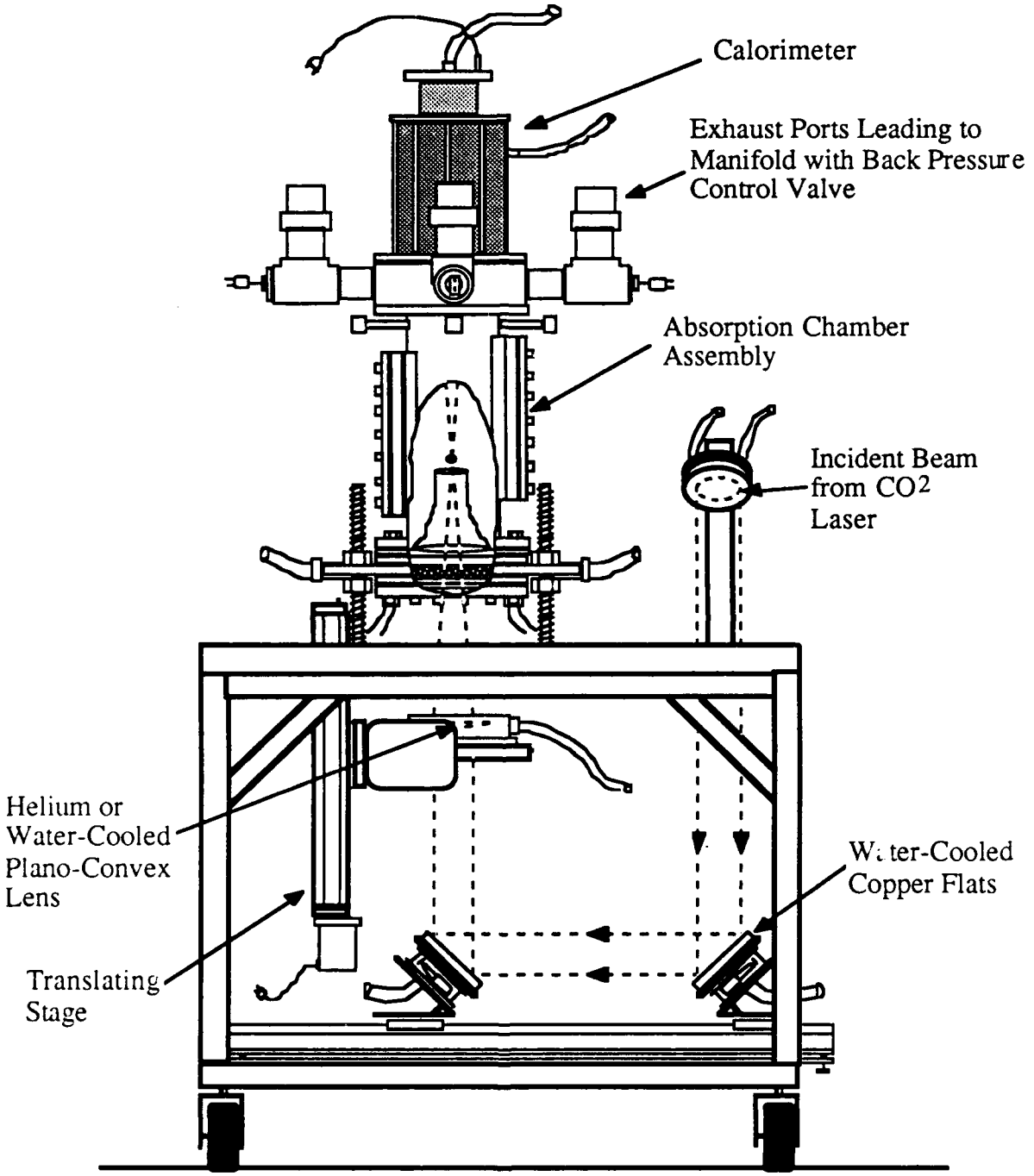

Figure 3.2 Schematic of the test stand highlighting positions of turning mirrors, lens, absorption chamber, exhaust ports, and calorimeter. Taken from Ref. 19.

the available power in the chamber to approximately 7 kW. The calibration method and errors involved are discussed in Chapter Four.

3.2. Absorption Chamber

After the beam has passed through the optics, it is focused into a 127 mm inside diameter (ID) stainless steel flow chamber. Gas is introduced into the bottom of the flow chamber through two half inch hoses. The gas enters an annular plenum with 24 exit holes that exhaust the gas into the chamber. Previously there was much turbulence associated with the introduction of the gas through these holes. This turbulence limited the possible mass fluxes by causing premature instabilities in the LSP's. In order to quiet this turbulence a sintered steel flow straightener with a 40 μm pore size was installed. This flow straightener quieted the flow substantially and allowed higher mass fluxes than previously possible [22].

Mounted just above the flow straightener is a converging section quartz tube as shown in Figure 3.3. The tube has an ID of 48 mm with a wall thickness of 3 mm and serves to accelerate the flow without blocking spectroscopic access to the plasma. Plasmas have been sustained at over 33 m/s using the quartz tube.

As mentioned previously a tungsten rod is used to supply free electrons and initiate a plasma. The tungsten insertion location is approximately 17 mm above the lip of the quartz tube. Side windows on opposite sides of the flow chamber allow visual access to the plasma and tungsten target. To monitor chamber wall temperature a type T thermocouple is embedded in the chamber wall. The flow chamber has been described in great detail elsewhere [1, 19, 20, 21, 22, 23, 24].

3.3. Gas Supply and Pressure Control Systems

Gas is supplied to the flow chamber via a long inlet hose connected to a group of five argon bottles outside the lab room. The gas is passed through a flow meter with an estimated error of ±3% based on the increments in the analog scale of percent maximum flow and increments in the back pressure gauge. Plasmas have been sustained with mass flow rates as high as 98.7 grams/second using this flow system. A second flow meter is used to add

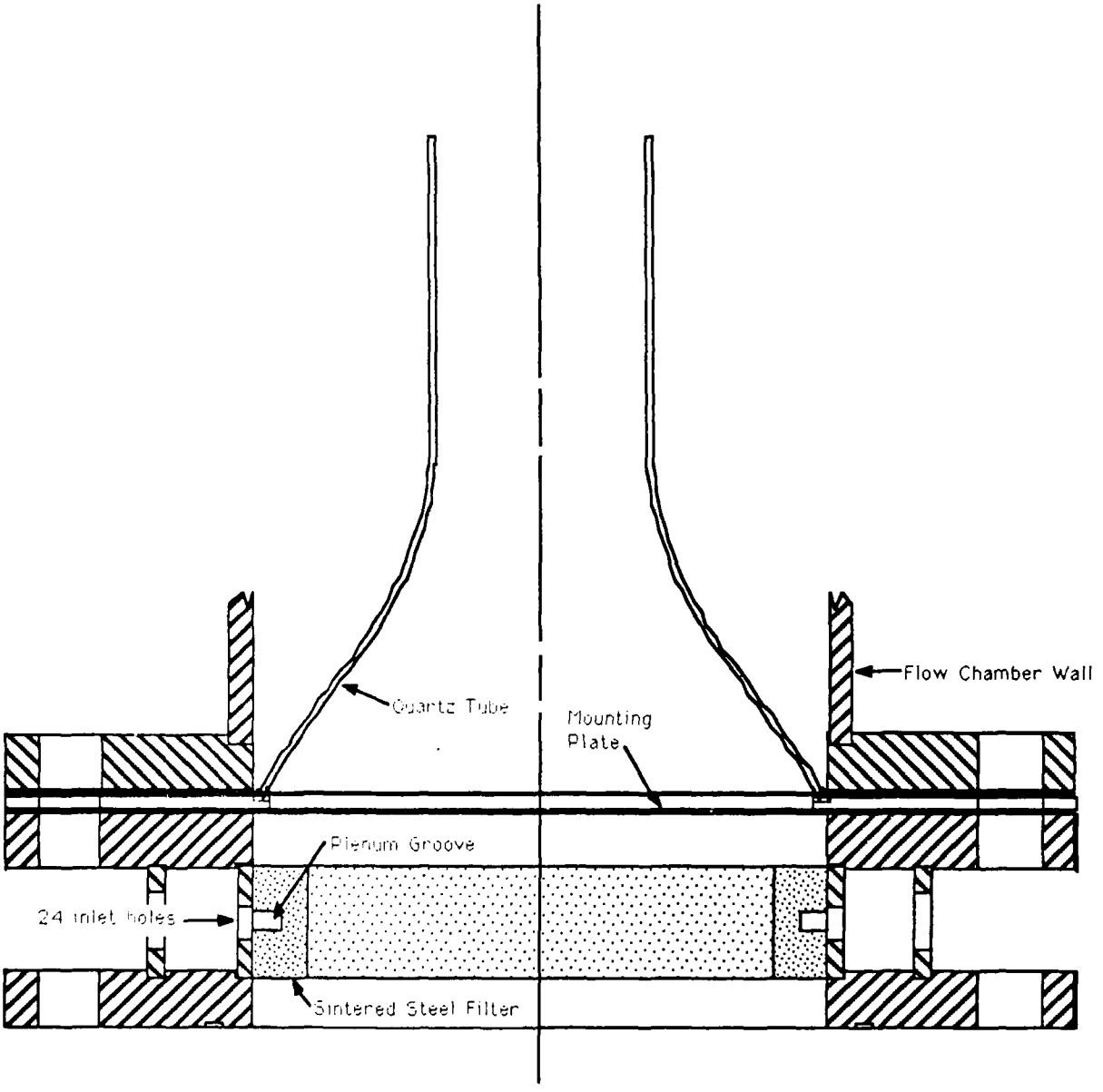

Figure 3.3 Schematic of inlet section showing converging quartz tube and sintered steel flow straightener.

helium during helium/argon mixture experiments.

The flow chamber has four half inch exit ports built into it near the top. Previously the possible mass flow rates to the flow chamber were limited by compressibility effects in the chamber exit ports and a corresponding pressure rise in the chamber itself. This made it impossible to separately study the effects of elevating the mass flux and elevating the pressure because the two effects were coupled [22]. The built in exit ports were capped and a new aluminum exit section was made which was then clamped to the top of the flow chamber. The exit section features four two inch tapped exit ports into which the exit piping system was threaded. One-eighth inch thick wet felt insulation from Refractory Products Company covers the entire inside surface of the exit section and extends out into the exit ports beyond the position of the thermocouples. The new insulated exit ports provide over twelve times the exit area compared to the old ports which means that over twelve times more mass can be passed through the system without causing the flow to become compressible. As with the old system, type K fast response thermocouples were positioned in each of the four exit ports. The wet felt insulation installed in each of the exit ports helps to prevent the hot argon gas from losing energy to the cold chamber walls via convection before the gas reaches the thermocouples.

3.4. Calorimeter

A watercooled copper cone calorimeter used both as a beam dump and to measure the amount of energy passing through the chamber is mounted to the chamber directly above the exit section. An array of thermocouples within the calorimeter measures the temperature difference of the cooling water between the outlet and inlet. This temperature difference is used to calculate the amount of power incident on the calorimeter. A failsafe system connected to the calorimeter cooling water control valve prevents plasma initiation (prevents target insertion) if the cooling water is not flowing at a minimum rate to protect the calorimeter. Calorimeter calibration and plasma global absorption determination are discussed in Chapter Four.

3.5 Fluke Data Acquisition System

All data is monitored and recorded with either a Fluke Model 2400B or a Model 2240A

Data Acquisition Computer. The Model 2400B recently developed problems in its operation and had to be replaced with the Model 2240A. Regardless of which model is used, the Fluke is connected to the inlet and exit thermocouples, calorimeter thermocouples, chamber pressure transducer and chamber wall thermocouple. All these inputs are scanned once every 1.5 seconds and this data is displayed on a screen and written to a file to be saved for data analysis. Data saved in this way is then uploaded to a Macintosh Plus computer located in Mechanical Engineering Laboratory room 212 and run through a data reduction code written by Scott Schwartz, a graduate research assistant. In addition, the lens translation system that is used to move the LSP to the desired position within the quartz tube is also controlled by the Fluke. A complete description of the Fluke hardware and software can be found in Reference 32.

3.6. OMA and Optical Diagnostics

The Optical Multichannel Analyzer (OMA) III system made by EG&G Princeton Applied Research (PARC) was utilized for the optical diagnostics of the laser-sustained plasmas. Figure 3.4 is a schematic of the experimental setup. The entire detection system is located in the experiment control room which can be seen in Figure 3.1. The system can be divided into three sections: first the plasma imaging optics and the spectrograph, second the optical multichannel analyzer system, and third the translation stages and stepping motor-controller assembly.

3.6.1 Plasma Imaging Optics and Spectrograph

A 3 inch diameter, 20 cm focal length ORIEL plano-convex lens was used to image the plasma onto the monochromator entrance slit. During the alignment process, it is important to make sure that the plasma and the monochromator slit are along the optical axis of the lens. This is done by the use of a HeNe laser beam and is detailed in the experimental procedures in Reference 23.

The plasma image entering the slit is expanded spectrally by a 0.32 meter coma corrected Czerny-Turner configuration HR-320 spectrograph/monochromator made by Instruments

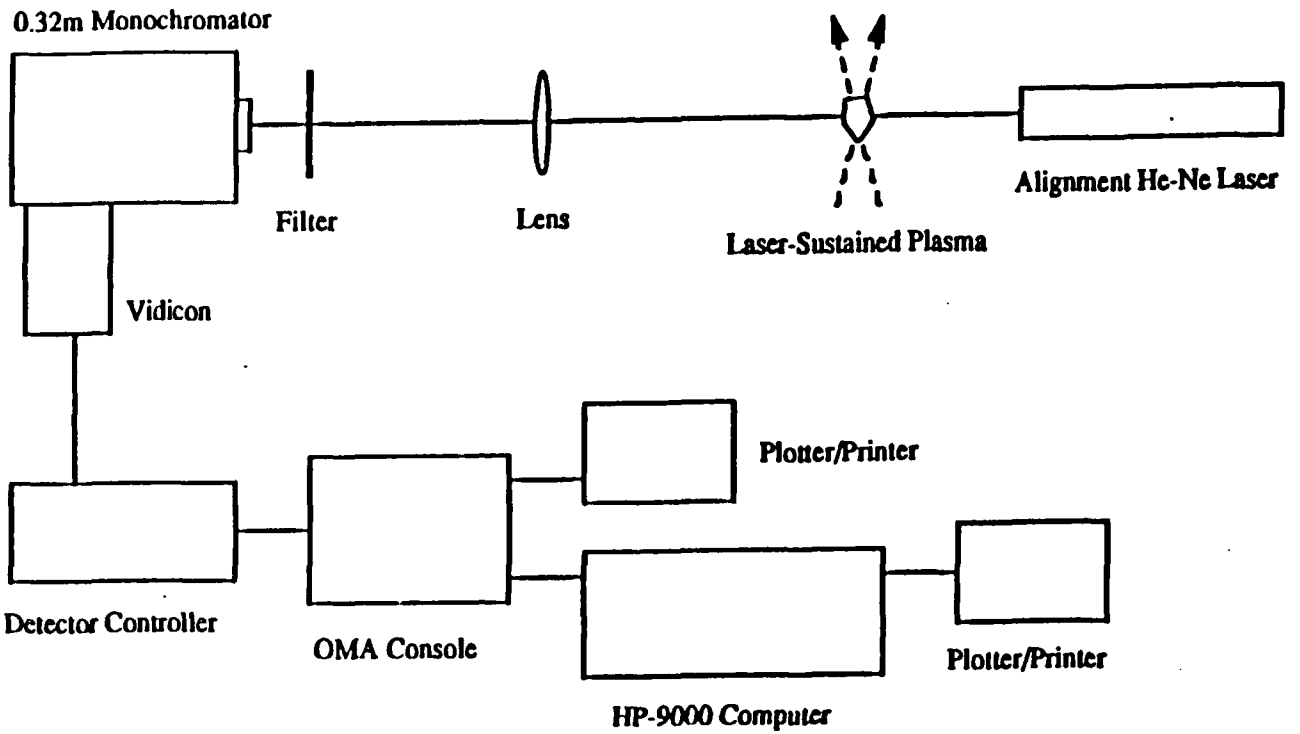

Figure 3.4 Schematic of the experimental setup including the OMA data acquisition and computer systems.

SA, Inc.. It is a rugged, compact instrument which is specifically designed to be operated either as a spectrograph when used with a vidicon or any solid state detector, or as a scanning monochromator when used with a photomultiplier tube (PMT) detector. Three 58x58 mm holographic gratings are available with groove densities of 147 g/mm, 1200 g/mm and 3600 g/mm for different dispersion needs. The 1200 g/mm grating which has a dispersion of 25 angstrom/mm (corresponding to a spectral coverage of about 250 angstroms at the exit port) with a resolution of 0.6 angstroms near the 415.8 nm ArI line was used in normal data acquisition.

The 147 g/mm grating has a larger spectral coverage, and thus can be used to observe the entire plasma radiation spectrum. The 3600 g/mm grating can be used to look into fine structures within the spectrum, since it has a greater dispersion.

Fixed slits were used at the monochromator entrance port. The slit used in this experiment is 8 mm long and 0.025 mm wide. Since the plasma emission is very strong, a narrow slit is used to take advantage of the better resolution. Neutral density filters have to be used in front of the entrance slit to cut down the light intensity to a safe level for the vidicon detector. A narrow slit will also help in this regard.

A radial "slice" of the plasma image enters the monochromator entrance slit. The grating then expands the image of the slit spectrally in the direction perpendicular to the slit. This forms a two dimensional optical output with one dimension corresponding to the plasma radial position, and the other the wavelength. This 2-D image is then projected to a vidicon detector surface where the optical signal is converted to a digitized voltage and stored for data reduction.

3.6.2 Optical Multichannel Analyzer

The EG&G Princeton Applied Research OMA III system consists of three parts: the Model 1460 OMA Console, the Model 1216 Multichannel Detector Controller, and the Model 1254 Silicon Intensified Target (SIT) Vidicon Detector.

The console is the unit which controls data acquisition, display and storage. Update software packages are provided by EG&G PARC using the keyboard and/or touch screen.

Various data acquisition modes and scanning sequences are available which include live, live minus background and accumulated intensities. The console also has a gated mode which requires the use of a Model 1211 High Voltage Pulse Generator. Data is immediately displayed on the console 9 inch screen and stored in either a 20 MB hard disk or a 150 K floppy disk. The console can communicate with other devices such as a printer, a plotter, or another computer through RS232 ports.

The 1216 Multichannel Detector Controller serves two purposes. First it accepts the scanning code from the console and drives the vidicon scanning sequence. Second it receives and digitizes the signal from the vidicon and sends it to the console for display and storage.

The SIT vidicon has a 12.5x12.5 mm detector surface composed of 512x512 pixels. These pixels can be grouped in different patterns and exposed for different time intervals. The vidicon detector is a light integrating device; charge stored on each detector element is depleted by incident photons and thermally freed electrons. At the end of the exposure (integration) period, the target is scanned by an electron beam that recharges the target elements. The variation in beam current as the target is scanned becomes the signal that is digitized in the detector controller. The vidicon has a sensitivity of approximately 2 detected photons/count with a linearity of ±2%, but is a function of intensity. The useful spectral range is from 365 nm to 800 nm but can be extended down to 200 nm with a UV scintillator coating.

3.6.3 Translation Stage and Stepping Motor-Controller

The plasma imaging optics, the monochromator and the vidicon are all mounted on a vertical translation stage, so that the whole assembly can be moved vertically to map out the entire plasma region "slice by slice". The vertical stage is positioned on another translation stage which provides horizontal movement of the detector system. This is particularly useful in locating the plasma at the center of the vidicon surface.

Chapter 4. Experimental Procedure and Data Analysis

4.1. Input Laser Power Calibration

The actual laser power that is available for initiating and sustaining plasmas within the absorption chamber is not the same as the laser power that is output by the laser due to optics losses as mentioned previously. These losses can be measured by generating a calibration curve of measured laser power versus laser detector voltage within the absorption chamber and in front of the test stand before the beam reaches the optics. The difference in the two measured powers is then the power lost in the optics through absorption and back reflections. Laser output power is controlled by the laser detector voltage which can be set by the laser operator and is displayed digitally on the laser control panel. Laser power is measured as described in Reference 24. It has been found that the laser power in front of the optics increases linearly with detector voltage. Incident power within the chamber versus detector voltage is slightly nonlinear due to increase of optics losses with incident power.

4.2. Initiation and Translation of LSP's

The tungsten target used for initiation can be extended into the chamber by the experimenter with a switch in the diagnostics room. Since the CO_2 laser operates in the infrared (10.6 μm), its beam cannot be seen. A visible (red) helium-neon laser concentric with the CO_2 laser is used to align the optics system and assure that the beam will strike the target. After the optics have been aligned, the argon gas is set to the desired flow rate with the flowmeter and the chamber pressure is adjusted with the valve handle hanging from the ceiling. The laser is turned on and the experimenter quickly inserts and retracts the tungsten rod into and out of the beam. If the system is aligned properly, initiation is practically instantaneous. The target cannot be extended to initiate a plasma unless a sufficient flow rate of water is flowing through the calorimeter to protect it from damage. Once the plasma has been initiated, it is translated down (usually 40 millimeters) into the quartz tube by translating the focusing lens via the Fluke system as described in Reference 32.

4.3. Inlet and Exit Port Thermocouples

The thermocouples used in this work have an intrinsic error of ± 0.75% as specified by the manufacturer, Medtherm Corporation. This error does not include errors due to gas compressibility or radiative losses which are discussed in Reference 24. The total thermocouple error can be summarized as follows. The intrinsic error associated with the thermocouples is ±0.75% per thermocouple (±0.375% for the average of four thermocouples). The error associated with gas compressibility can be estimated as less than ±0.5% although there is still a question as to the behavior of the inlet PVC plenum thermocouple [24]. Errors associated with radiation and convection losses are assumed to be small. Accounting for all sources of error, a good estimate of the total thermocouple error is less than ±1% per measurement [24].

4.4. Global Absorption Measurements

As defined in Chapter One the global absorption is the percentage of input laser power that is absorbed by the LSP. This percentage is determined by subtracting the power that is transmitted through the LSP to the calorimeter from the incident power and dividing by the incident power. The watercooled calorimeter is calibrated as described in Reference 24. Errors associated with calorimeter measurements can be grouped as those caused by errors in the calibration, those caused by heated gas within the chamber exchanging heat with the calorimeter, and those caused by scattering of the laser radiation and plasma irradiation of the calorimeter. Errors inherent to the calibration include the input power uncertainty (±3%) as well as the uncertainties in the array of thermocouples (±0.5 K per thermocouple) and the water flow rate in the calorimeter (±4%). The error in the measured incident power due to the calibration is therefore calculated to be approximately ±0.10 kW by the method of Reference 33. Errors due to hot gases (which would cause artificially high power measurements) have been found to be less than 3% [22]. Errors due to laser scattering and plasma irradiation are assumed to be negligible. Accounting for all sources of error, a good

estimate for the total calorimeter incident power measurement error is approximately ±0.13 kW per measurement [24].

A typical plasma experiment is allowed to continue until the displayed calorimeter power levels off to a constant value. The Fluke data acquisition system scans and records the calorimeter power once every 1.5 seconds. The data reduction code averages all data over eight scan intervals to smooth any random fluctuations. This averaging of data also reduces uncertainties. Once the power incident on the calorimeter has been determined, the global absorption is determined by the simple relation:

$$\% \alpha = \frac{P_{input} - P_{measured}}{P_{input}} \tag{4.1}$$

The total error in the measured global absorption can then be calculated to be less than ±4% [24].

4.5. Thermal Efficiency Measurements

The thermal efficiency was defined as the percentage of input laser power retained by the gas as thermal energy. The temperature rise of the gas flowing through and around the plasma as measured by the method previously discussed is recorded once every 1.5 seconds by the Fluke. The data reduction code averages these temperatures over 8 scan intervals to smooth any random fluctuations. Thermal efficiency is then determined by the following relation:

$$\% \eta = \frac{\dot{m} C_p \Delta T}{P_{input}} \tag{4.2}$$

where $\dot{m}$ is the mass flow rate, C_p is the constant pressure specific heat, ΔT is the temperature rise and P_{input} is the input laser power.

Errors associated with the thermal efficiency are due to the mass flow rate uncertainty (±3%), the temperature difference uncertainty (less than ±4% for average exhaust temperatures greater than 340 K), and the input laser power uncertainty (±3%). The total error in the measured efficiency can therefore be estimated as less than ±6% by the method of Reference 33.

4.6. OMA Alignment and Operation

System alignment is the first and the key procedure for obtaining reliable experimental results. The OMA alignment procedure is fully described in Reference 23. Normal data acquisition procedures will be described following a brief explanation of the OMA system operations. Finally the data reduction procedure will be detailed in its own sequence: the calculations of electron temperature, total plasma absorption and radiation loss, and the system thermal efficiency.

The two dimensional vidicon detector surface consists of 512x512 pixels. Because of the drop off in response at the outer 10% of the detector surface, X and Y are usually limited to the central region of the detector surface. The X parameter is called the channel. The range of the X parameter can be changed by setting the value of the first channel and the total number of channels. This enables the experimenter to manage the spectral range to be scanned. The pixels in the Y direction have to be grouped in tracks with a minimum of 5 elements in each track to eliminate error.

Channel time is defined as the variable time interval between 20 msec and 140 msec during which a scanned channel is exposed to a light signal. Due to strong signals from the plasma emission, the shortest channel time was used. Track time and frame time are the time intervals during which one track or the whole scanned area is exposed. When using the accumulative data acquisition mode, the experiment time indicates the time necessary to scan and add a series of exposures and preparation scans, the pattern of which is previously programmed. For a typical laser-sustained plasma, experiment time is 4 to 9 seconds.

Once data is obtained, it can be assigned a file name and stored in either the hard disk or a floppy disk. The OMA system is capable of doing the first few steps of data reduction, such as channel profile (integration) and curve calculations.

4.6.1. Data Acquisition

All the data in this work was acquired using the OMA data acquisition mode #6 in which intensities from subsequent data scans are added with several preparation scans in between.

The preparation scans are detector scans without light exposure, which are intended to eliminate dark signals. The monochromator center wavelength was adjusted to 422.0 nm and the range is large enough to include the 415.8 nm and 422.0 nm ArI lines.

The vertical translation stage was controlled through a BASIC program which enables the monochromator/detector assembly to move up or down in equal step sizes. Vertical increment of DZ = 2 mm was used in this work.

4.6.2. Data Reduction

The first data reduction process is the preliminary reduction on the OMA console, which generates the 415.8 nm ArI line and continuum intensity distribution files. In order to calculate total absorption and thermal efficiency, laser beam geometry must be determined using a Laser Beam Analyzer (LBA) as described in Reference 23. Once the beam geometry is known, files can then be sent to an HP-9000 computer for further processing which yields temperature distributions, total absorption and thermal efficiency.

The intensities measured by the OMA are of line-of-sight integrated emission, which need to be inverted into local emissive power before being applied to the temperature calculations. The calculation of local emissive power from measured intensities is done using a process called Abel inversion which assumes a cylindrical symmetry. In most cases, plasma emission intensities appeared quite symmetric about the centerline, hence one half of the curve was chosen for the inversion. Averages were used in a few occasions when the symmetry was not very good. The line and continuum intensity files were then sent to an HP-9000 computer for further data reduction.

The Abel inversion code from Reference 6 was used to obtain local emissive powers from both the line and the continuum data files. Then the ratio was compared with theoretical results to get the local electron temperature. The final result was a two dimensional temperature field T(z,r), with z and r being the axial and radial positions respectively.

The CO_2 input laser beam was divided into 20 rays, each having a slightly different angle of incidence determined from the beam analysis described in Reference 23. Each ray

propagated through the temperature field, and the amount of power absorbed was summed along the beam path on a point-by-point basis. Total power absorbed was then obtained by adding the contributions from all the 20 rays. Dividing the absorbed power by the incident laser power yielded the fractional absorption.

The total radiation loss has to account for contributions from every point of the plasma. Hence it is an integration over the entire volume of the plasma. Again, the local radiation loss is a function of electron temperature which has already been determined. Power retained by the flowing gas is then the difference between the absorbed and radiated power. System thermal efficiency has been defined as the fraction of the incident laser power that was converted into thermal energy of the gas. A complete listing of the code that was used for the Abel inversion, total absorption and thermal efficiency calculations can be found in Reference 6.

Chapter 5. Discussion of Results

Laser propulsion is based on the conversion of electromagnetic energy of a laser beam to thermal energy of a propellant gas via a LSP. The goal of this work is to characterize the effects of several parameters on the efficiency of energy conversion and to gain an understanding of the physical processes involved. The parameters (including input laser power, gas mass flux, beam focusing geometry, and gas pressure) directly affect the size, shape, equilibrium position, and stability of a LSP, and therefore directly affect the thermal conversion efficiency. Physical understanding of the effects of these parameters for the moderate power levels available in the laboratory is the basis for extending results to the very high powers that will be used in practice.

Experiments to determine thermal efficiency and global absorption in pure argon were conducted for three laser input powers (2.5, 5.0, and 7.0 kW), two beam geometries (f-4.1 and f-7.1), two pressures (1.0 and 2.5 atmospheres), and a range of mass fluxes from 3.0 to over 50 kg/m^2s. Thermal efficiency varied from 11% to 46%, and global absorption varied from 55% to 97% depending on operating conditions. The effects of power, pressure, f-number, and mass flux on plasma size, shape, stability, global absorption and thermal efficiency of pure argon plasmas will be discussed.

Thermal efficiency and absorption measurements were also performed on plasmas created in flowing helium/argon gas mixtures. The manner in which these experiments were carried out was very similar to the experiments performed with pure argon plasmas. Helium was added to the argon in an attempt to foresee results of future experiments involving hydrogen, based on the similar specific heat, thermal conductivity, electron-atom elastic collisional cross-section, and molecular weight of helium and hydrogen. Helium, however, does not follow the absorption and emission coefficient trends of hydrogen as closely as argon does. Also the ionization energy of helium is much greater than that of argon and hydrogen (25eV compared to approximately 15eV for both argon and hydrogen). Since helium has a greater ionization energy than argon, a helium/argon plasma is first stabilized in pure argon and helium is then

added to the flow. The mixture fractions quoted in this study are therefore reported as the molar or volume percentage helium within the gas, the balance being argon.

In Chapter 1 gas velocity was used as a parameter to explain plasma stability. As long as only one type of gas at a given pressure is considered, gas velocity is an acceptable comparison parameter. However if the gas pressure is changed or if a mixture of gases is used, the gas velocity will also change for the same mass flow rate. Therefore comparing thermal efficiencies for two different pressures or compositions at the same gas velocity is meaningless. *The correct parameter to use for pressure comparisons is mass flux which is the product of gas velocity and density. The correct parameter to use for gas mixture comparisons is mole flux.* It should be noted that the mass flux for a single gas plasma can easily be converted to a mole flux by multiplying by a constant.

In addition to thermocouple and calorimeter data, filtered photographs of several plasmas were taken for the relative comparison of plasma size, location, and shape at various operating conditions. Spectroscopic measurements of plasma emissions were also recorded for several operating conditions. The results for pure argon plasmas will be discussed first, followed by results for helium/argon mixture plasmas. Finally, assumptions and algorithms used in the UIUC two-dimensional numerical model will presented and results will be compared with experimental results.

5.1. Power Effects

The laser input power determines the power density of the focused beam. Raising the laser input power will cause the plasma wave front to move upstream away from the focus to a region of the beam where the power density again balances convective and radiative losses. This effect is clearly seen in Figure 5.1 which is a comparison of a 2.5 kW and a 5 kW plasma at the same f-number, pressure, and mass flux.

As discussed in Chapter 1, a LSP will become unstable if the gas mass flux is so high that the beam power density (even at the focus) is insufficient to balance total losses. In this event the LSP is pushed downstream of the focus where it extinguishes (referred to as a plasma

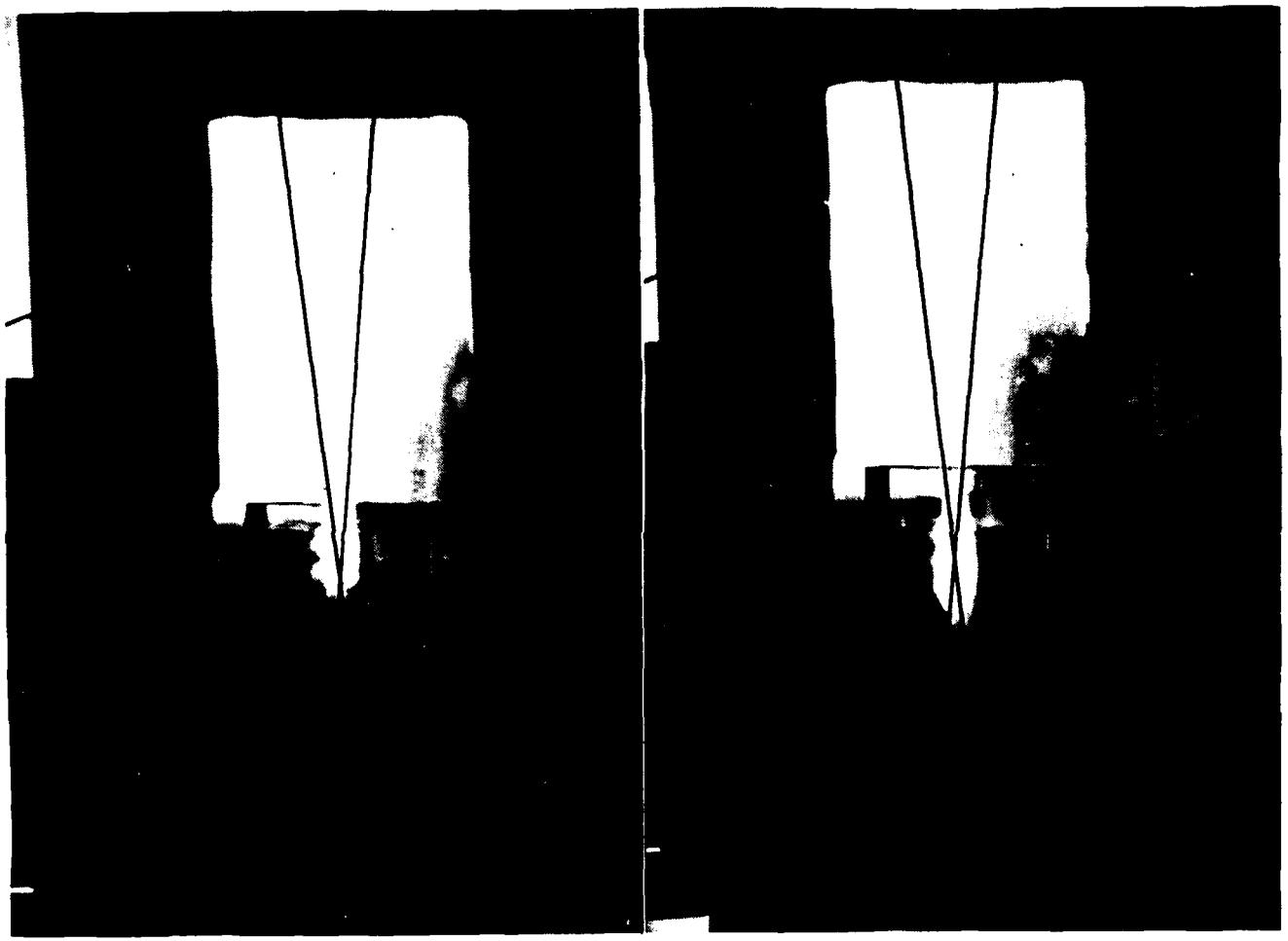

Figure 5.1 Double exposure photographs of a 2.5 kW, 1 atm., f-4.1, 3.1 kg/m^{2}s pure argon LSP (left) and a 5 kW, 1 atm., f-4.1, 3.0 kg/m^{2}s pure argon LSP (right). The beam focusing geometry has been superimposed on the photographs for clarity and to show the position of the focus. Note that the 5 kW LSP is further upstream (lower in the tube and farther from the focus), and also slightly larger.

blowout). Since raising input power causes the LSP position to shift upstream, a higher mass flux will be necessary to push the plasma through the focus and cause a blowout. In order to determine the upper mass flux limit at which 1 atmosphere plasmas could be maintained, a series of blowout mass flux experiments were conducted using the f-7.1 NaCl lens and a ZnSe window. Typically, a primary data point was acquired by first stabilizing a low mass flux plasma at a given power and then slowly increasing the mass flux until the plasma extinguished. Three such acquired data points would then be averaged to produce a final data point. As the blowout mass flux is approached, the plasma typically begins to oscillate due to small random variations in flow conditions and input power. The amplitude of this oscillation increases with mass flux until the plasma extinguishes.

The mass flux at which a plasma extinguishes should not be taken as absolute and could be better described by a range of possible blowout mass fluxes. Variations of power distribution in the annular input beam as well as small changes in the flow system will affect blowout mass flux. Therefore the results shown in Figure 5.2 should be taken as an indication of qualitative behavior and not as absolute quantitative behavior.

Raising the input power will also cause the plasma to become slightly larger, as can be seen in Figure 5.1. The larger 5 kW plasma intercepts a longer beam path than the 2.5 kW plasma, and the 5 kW beam has a higher power density than the 2.5 kW beam. These two factors result in a larger (and hotter) plasma with increased power which results in an increase in global absorption at the same mass flux.

Since the 5 kW plasma is larger and hotter than the 2.5 kW plasma, radiation losses will also be higher. Although the 5 kW plasma has a higher global absorption, its higher radiation losses cause the thermal efficiency to be lower than that of a 2.5 kW plasma at the same mass flux. The higher global absorption and lower thermal efficiency at the same mass flux as well as higher blowout mass flux with increased input power can be seen in the data plotted in Figure 5.3.

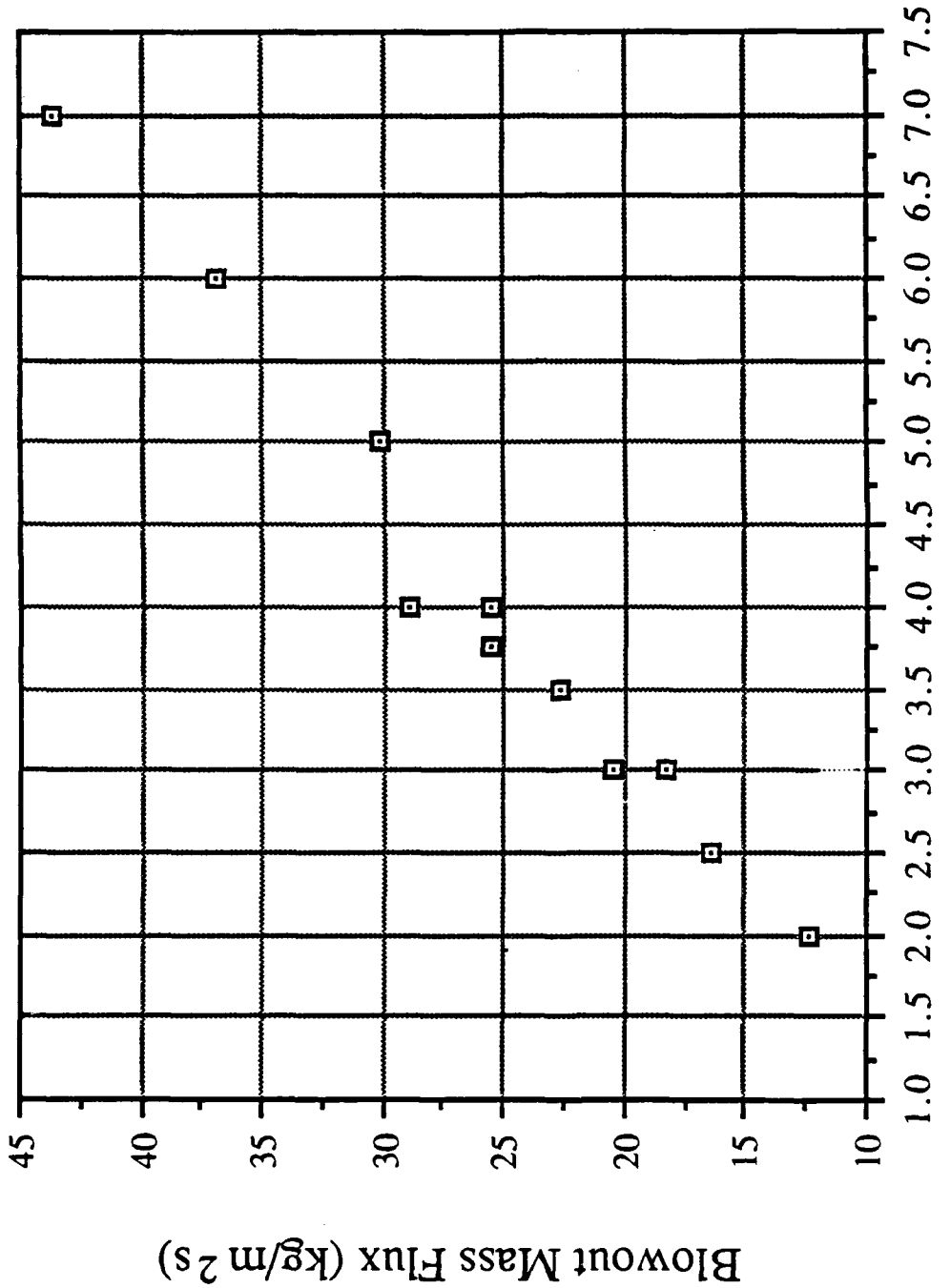

Figure 5.2 Blowout mass flux versus input laser power for pure argon LSP's.

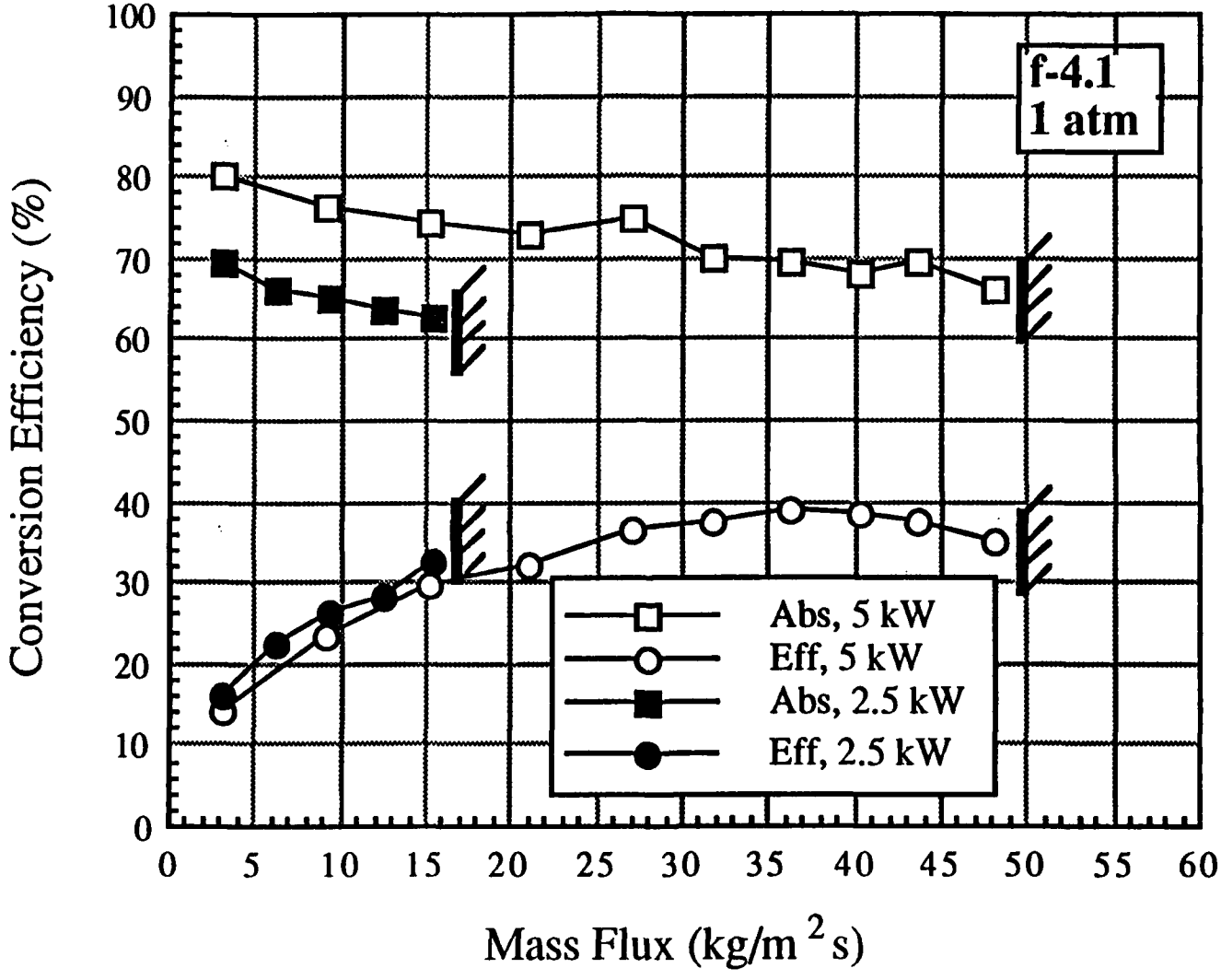

Figure 5.3 Comparison of global absorption and thermal efficiency data for f-4.1, 1 atm. pure argon LSP's at 2.5 kW and 5 kW laser input power. Walls superimposed on figure denote LSP stability mass flux limits. Note decreasing absorption for both powers with mass flux and peak in thermal efficiency for 5 kW LSP's.

Although the 5 kW plasmas had lower thermal efficiencies than the 2.5 kW plasmas for the same mass fluxes, the 2.5 kW plasmas became unstable much sooner. Referring to Figure 5.3, the 2.5 kW plasmas could not be maintained beyond approximately 16.6 kg/m^{2}s whereas the 5 kW plasmas remained stable to beyond 48 kg/m^{2}s. Thus if the entire range of stable plasmas is considered, the 5 kW plasmas achieved a higher thermal efficiency than the 2.5 kW plasmas, and, in general, plasmas of higher power can achieve higher thermal efficiencies.

5.2. Pressure Effects

Since gas pressure is a measure of the number density of the gas, it is also related to the number of free electrons at a given temperature. The absorption coefficient for a LSP increases with the number of free electrons present, and therefore with the gas pressure. The relation between absorption coefficient and electron number density is given by the expression:

$$\alpha(m^{-1}) = \frac{4}{3} \frac{2\pi e^6 \bar{Z} N_e^2 \lambda^3}{(6\pi k m_e^3 T_e)^{1/2} hc^4} \left[1 - \exp(-h\upsilon/kT_e) \right] (g_{ff} + \frac{h\upsilon}{kT_e}) \qquad (5.1)$$

where T_e and N_e are the electron temperature and number density respectively, Z the effective ion charge and g_{ff} the free-free Gaunt factor.

The effect of a higher absorption coefficient is to cause the LSP to move upstream to a region of lower beam power density. A comparison of two plasmas with similar mass fluxes at 5 kW with an f-4.1 beam geometry for 1 and 2.5 atmospheres pressure is shown in Figure 5.4. Note that in addition to being further upstream, the 2.5 atmosphere plasma is also much smaller. This size difference is due to the higher absorption coefficient at 2.5 atmospheres. The incoming beam gets absorbed in a shorter beam path which results in a smaller plasma.

At low mass fluxes the global absorption of a 2.5 atmosphere plasma is less than that of a comparable 1 atmosphere plasma. However, as mass flux is increased, the 2.5 atmosphere plasma absorption overtakes that of the 1 atmosphere plasma and continues to increase as can

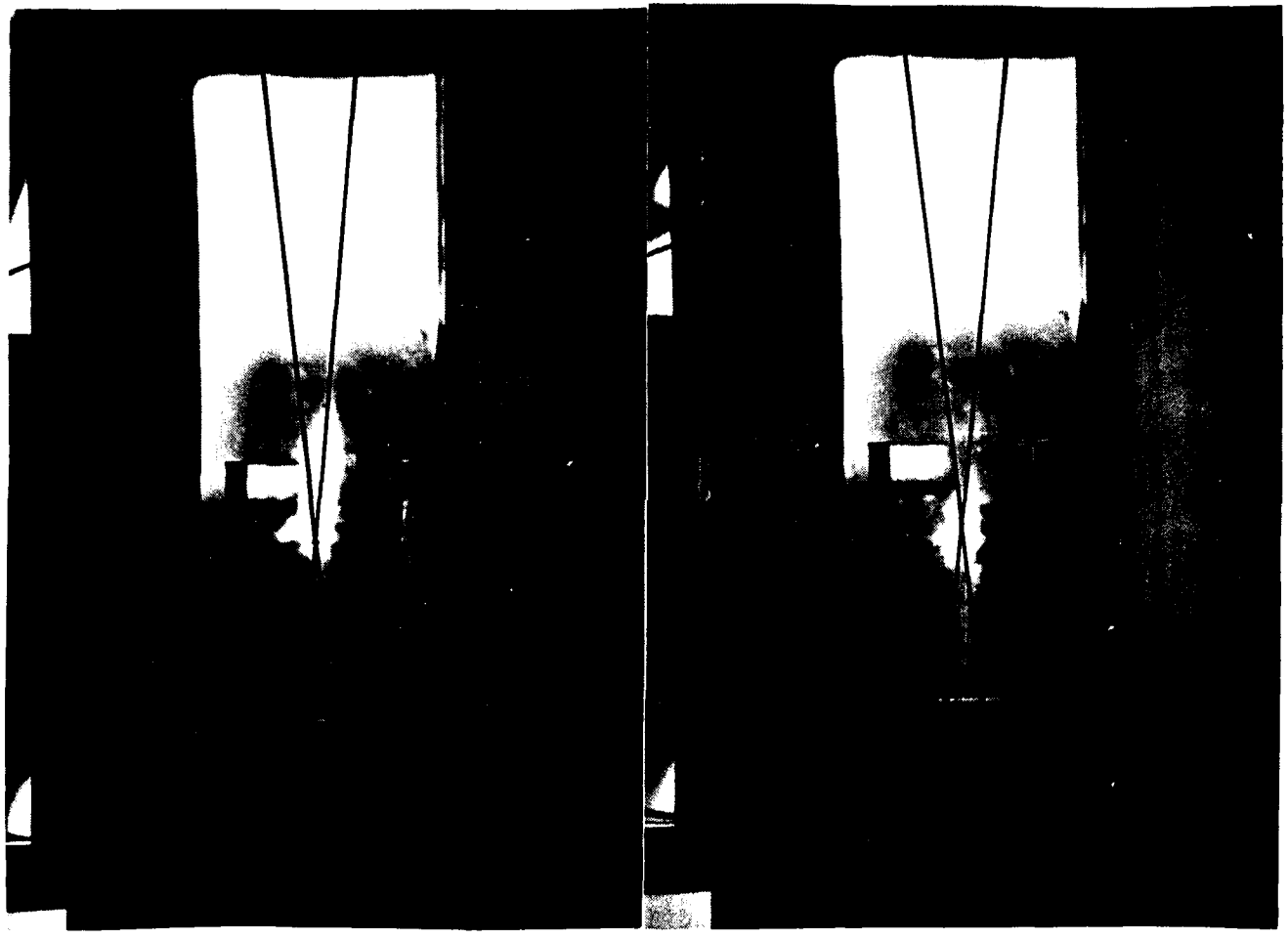

Figure 5.4 Double exposure photographs of a 1 atm., 5 kW, f-4.1, 48.1 kg/m^{2}s pure argon LSP (left) and a 2.5 atm., 5 kW, f-4.1, 46.6 kg/m^{2}s pure argon LSP (right). The beam focusing geometry has been superimposed on the photographs for clarity and to show the position of the focus. Note that the 2.5 atm. LSP is further upstream (lower in the tube), and much smaller.

be seen in the data plotted in Figure 5.5. This behavior is due to the positions of the plasmas in the focused beam relative to the beam focus. At low mass fluxes the 2.5 atmosphere plasma is far upstream of the focus in a low power density region of the beam. This region of the beam can be thought of as a relatively cool region. At the same mass fluxes, the 1 atmosphere plasma stabilizes nearer to the focus in a region of higher beam power density (a hotter region of the beam). The closer proximity of the 1 atmosphere plasma to the beam focus results in a hotter plasma with a higher global absorption.

As mass flux is increased, the 2.5 atmosphere plasma is pushed downstream closer to the focus while the 1 atmosphere plasma is pushed through the focus. Now both plasmas intercept the beam near the focal region, but since the 2.5 atmosphere plasma has a higher absorption coefficient than the 1 atmosphere plasma, its global absorption overtakes that of the 1 atmosphere plasma. Eventually as the mass flux is increased further the 1 atmosphere plasma becomes unstable and blows out while the 2.5 atmosphere plasma gets pushed through the focus and its global absorption continues to increase. The highest recorded global absorption using pure argon was 97% for a 2.5 atmosphere, f-4.1, 5 kW plasma at approximately 51 kg/m^2s which can be seen in Figure 5.6.

Thermal efficiency is lower for the 2.5 atmosphere plasma than for the 1 atmosphere plasma for the same mass flux for reasons previously outlined. At low mass fluxes a 2.5 atmosphere plasma absorbs less of the incident beam. Although it also radiates a smaller percentage of its absorbed power, the retained power of a 2.5 atmosphere plasma is lower for these mass fluxes. At higher mass fluxes, a 2.5 atmosphere plasma absorbs more but also radiates more than a 1 atmosphere plasma resulting again in a lower thermal efficiency. The lower thermal efficiency of a 2.5 atmosphere plasma for any given mass flux can also be seen in Figure 5.5.

As with the case of a power increase, a higher mass flux would be necessary to push a 2.5 atmosphere plasma downstream towards a blowout instability than would be required for a 1 atmosphere plasma. In fact, none of the 2.5 atmosphere test cases could be made to blow

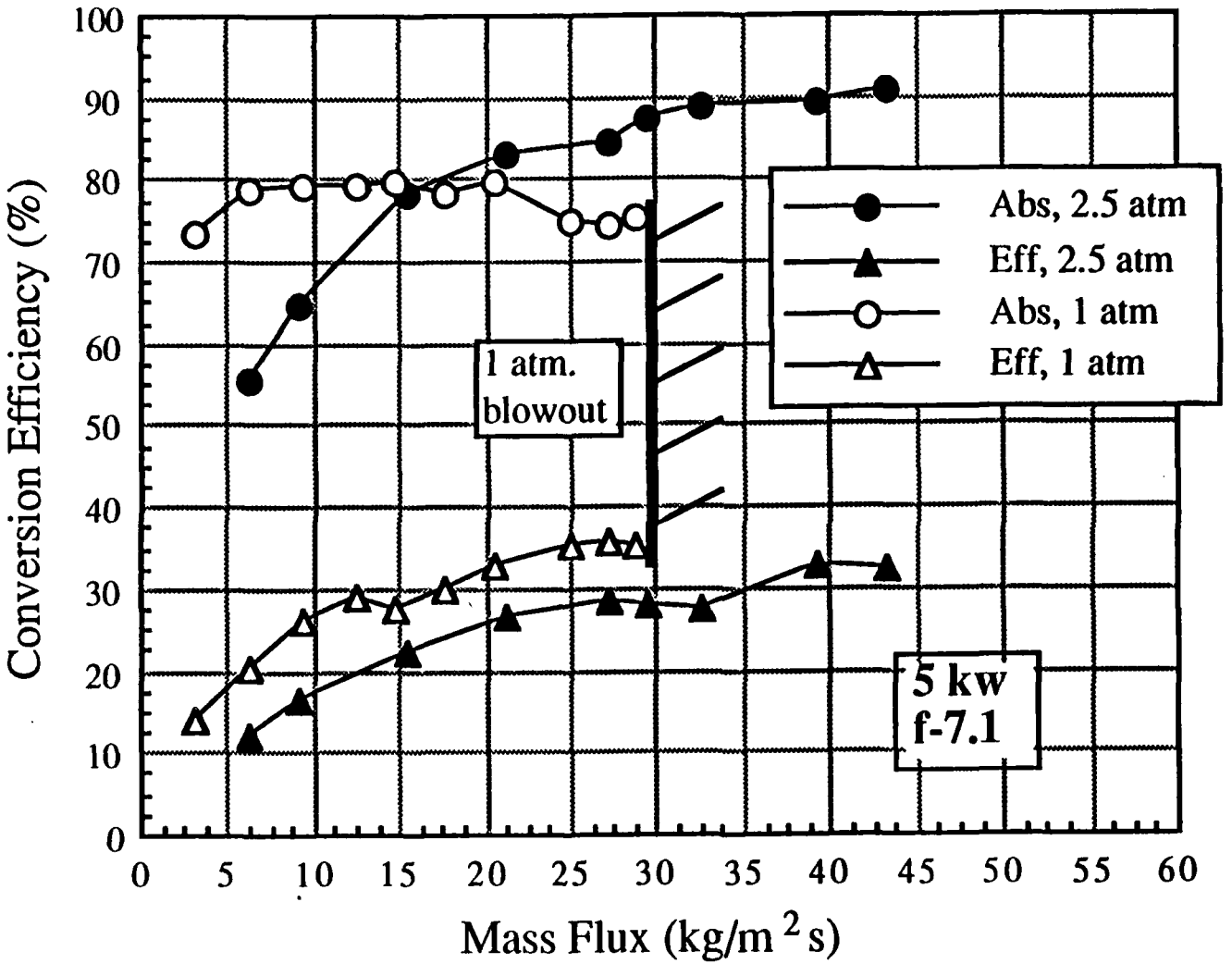

Figure 5.5 Comparison of global absorption and thermal efficiency for pure argon f-7.1, 5 kW LSP's at 1 atm. and 2.5 atm. gas pressure. Large wall superimposed on figure denotes 1 atm. LSP stability mass flux limit. Note that absorption and efficiency both appear to still be increasing with mass flux at the high end for the 2.5 atm. LSP's.

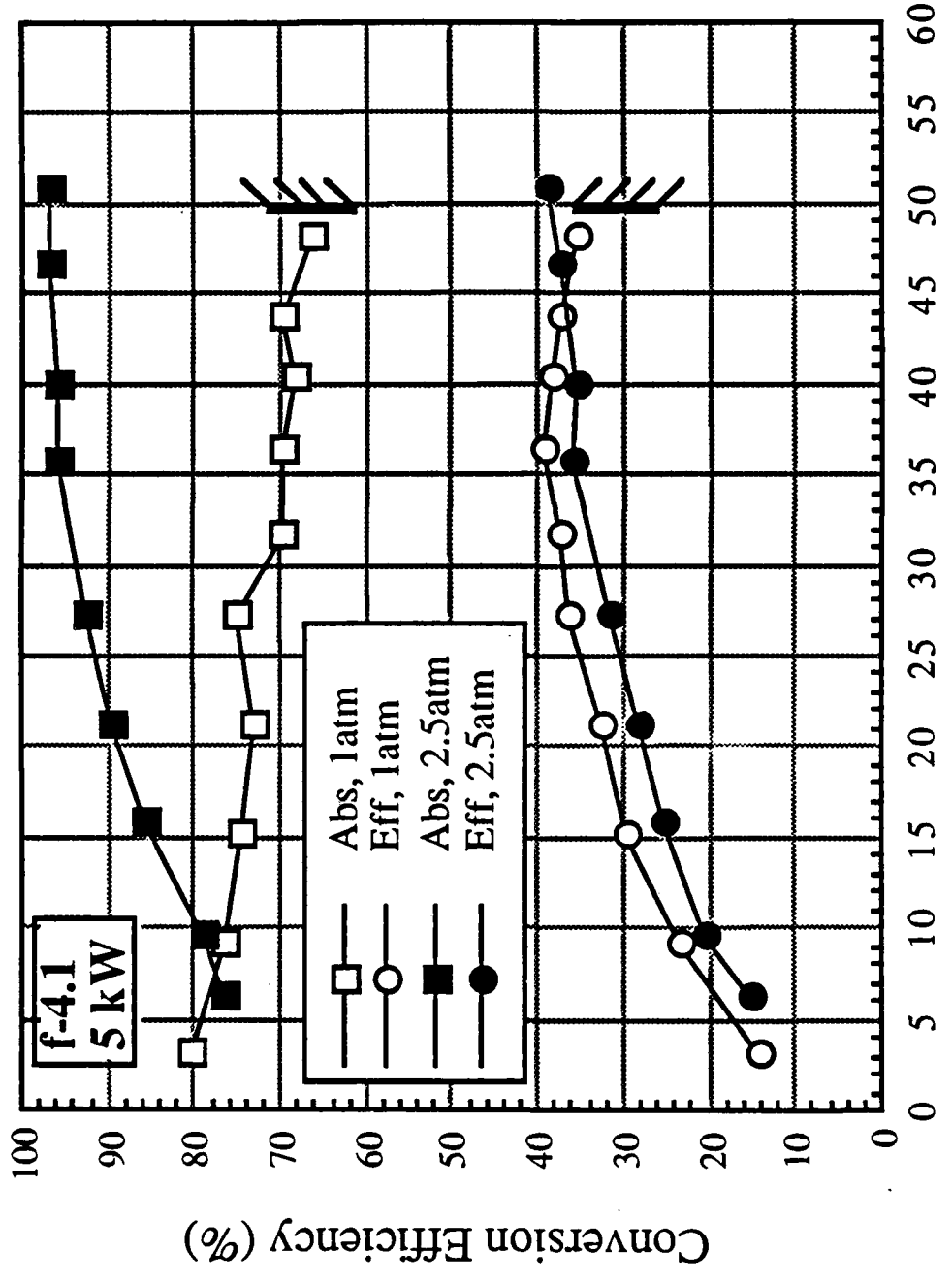

Figure 5.6 Comparison of global absorption and thermal efficiency for pure argon f-4.1, 5 kW LSP's at 1 atm. and 2.5 atm. gas pressure. Walls superimposed on figure denote 1 atm. stability mass flux limit. Note that the 1 atm. efficiency peaks at ~36 kg/m^{2}s while the 2.5 atm. efficiency continues to rise.

out even with the highest possible mass flux that the gas supply system could deliver, 54.5 kg/m^{2}s.

As can be seen in Figures 5.6 and 5.7, if the mass flux of a given 2.5 atmosphere plasma is increased beyond the blowout mass flux for a comparable 1 atmosphere plasma, the thermal efficiency of a 2.5 atmosphere plasma can exceed the maximum possible thermal efficiency at 1 atmosphere. This effect was also seen to accompany a power increase and will be explained in the section concerning mass flux effects, section 5.4.

In addition to instabilities at the higher mass fluxes previously referred to as blowouts, instabilities in 2.5 atmosphere plasmas were also noted at low mass fluxes. In particular it was not possible to sustain 2.5 kW, f-7.1, 2.5 atmosphere plasmas at mass fluxes below 15.5 kg/m^{2}s. At these flow rates the plasma is far upstream of the focus in a region of the beam that has a low power density. A small perturbation of either the mass flux or the input power would cause the plasma to drastically change position to match conditions, especially using an f-7.1 focusing geometry. If the position of the plasma cannot adjust quickly enough to these perturbations, the plasma will extinguish. This type of instability (associated with high f-numbers) has also been noted by Fowler [11] and Keefer [14].

5.3. F-Number Effects

Varying the f-number of the focusing optics changes the spatial rate at which the beam focuses. An f-4.1 beam focuses faster spatially than an f-7.1 beam, which means that at the same distance from the focus for each geometry and a given input power, the f-7.1 beam willhave a higher power density than the f-4.1 beam. If the region of each beam having the same power density is considered, then the region of the f-4.1 beam having a given power density will be closer to the focus than the corresponding region for the f-7.1 beam. Therefore, an f-4.1 plasma will stabilize closer to the focus than an f-7.1 plasma if all other flow conditions are the same (i.e. power, pressure, and mass flux) as can be seen in Figure 5.8 which is a comparison of an f-4.1 plasma and an f-7.1 plasma at nearly identical conditions.

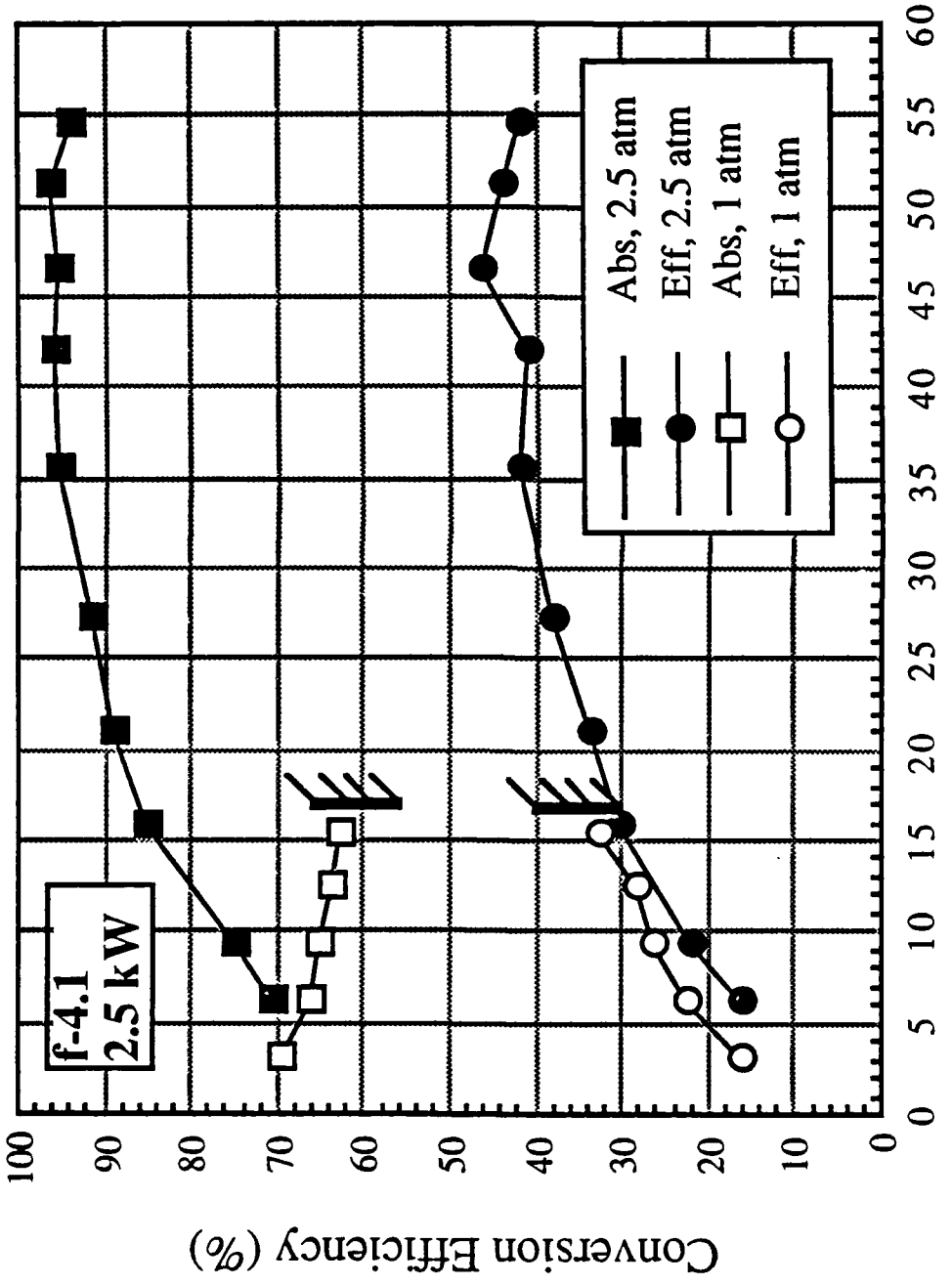

Figure 5.7 Comparison of global absorption and thermal efficiency for pure argon f-4.1, 2.5 kW LSP's at 1 atm. and 2.5 atm. gas pressure. Walls superimposed on figure denote 1 atm. stability mass flux limit. Note peak in thermal efficiency of 46% for 2.5 atm. LSP's.

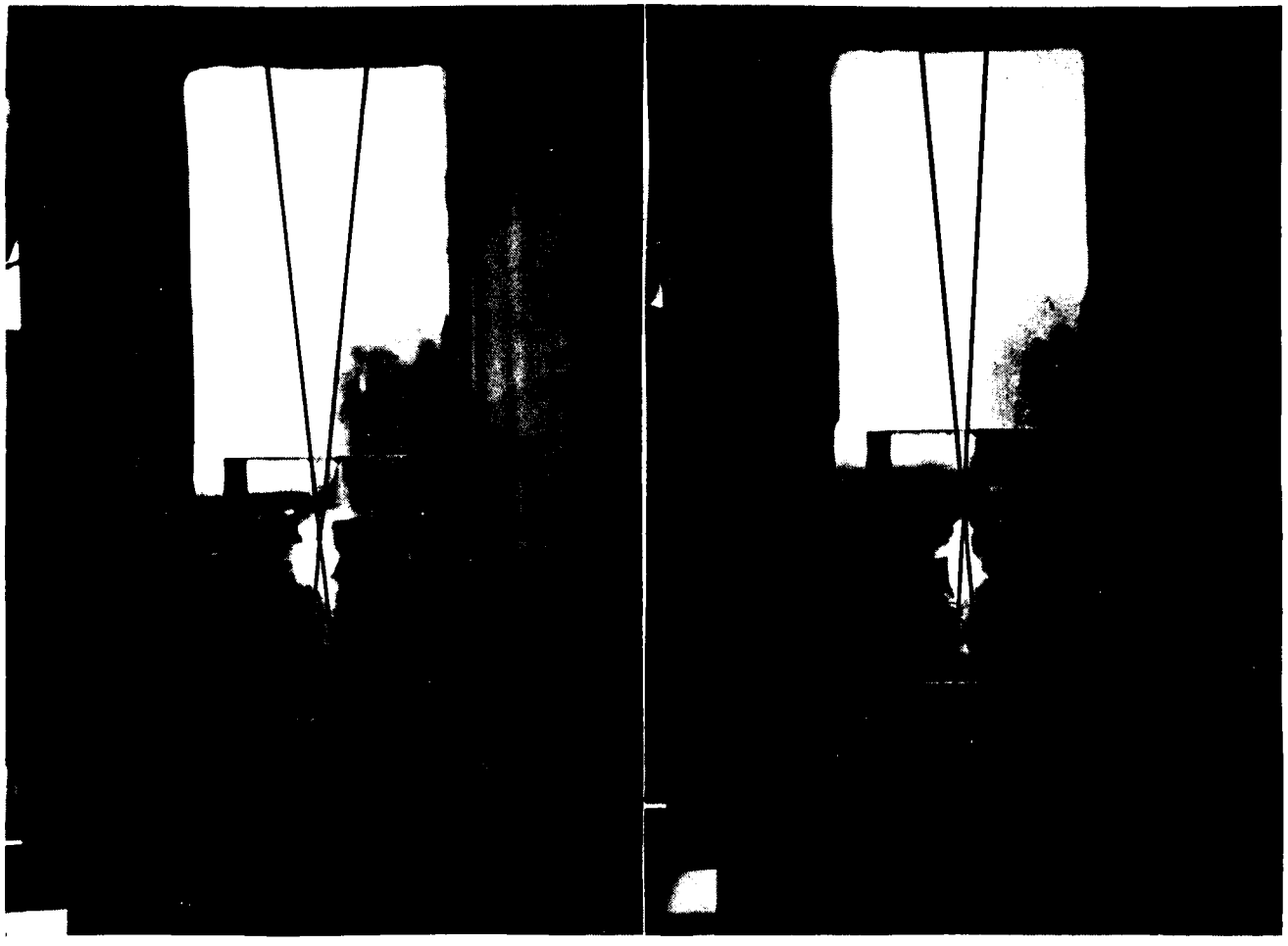

Figure 5.8 Double exposure photographs of an f-4.1, 2.5 kW, 2.5 atm., 15.9 kg/m^{2}s pure argon LSP (left) and a f-7.1, 2.5 kW, 2.5 atm., 16.5 kg/m^{2}s pure argon LSP (right). The beam focusing geometry has been superimposed on the photographs for clarity and to show the position of the focus. Note that the f-4.1 LSP is further downstream (higher in the tube and closer to the focus), and also appears thicker.

This implies that the f-4.1 plasma will stabilize closer to the hot focal region than the f-7.1 plasma which will stabilize farther upstream in a colder region of the beam even though the power densities at each plasma front are the same. The result is that the f-4.1 plasma intercepts a hotter region of the beam and has a higher global absorption for the entire range of mass fluxes, as can be seen in the data of Figures 5.9 and 5.10.

This result does not hold true for plasmas at 1 atmosphere pressure. As can be seen in Figure 5.11, the global absorption at 1 atmosphere pressure is higher for f-7.1 plasmas. The reason for the reversal in global absorption may be that the f-7.1 plasma intercepts a longer beam path than the f-4.1 plasma although this is not proven.

Referring to Figures. 5.9 and 5.10, thermal efficiencies of f-4.1 plasmas are slightly higher than those for f-7.1 plasmas at the same mass fluxes at 2.5 atmospheres pressure. However at 1 atmosphere pressure measured thermal efficiencies for similar mass fluxes are practically identical as can be seen in Figure 5.11. If the overall range of mass fluxes is considered (Figure 5.11) it can be seen that the f-4.1 efficiency continues to rise for mass fluxes beyond the f-7.1 blowout mass flux. The behavior of thermal efficiency with f-number is difficult to explain at either pressure but the trend of higher efficiency with lower f-number can be seen at both pressures.

A most striking effect of f-number is the large difference in the mass flux required to produce a plasma instability (blowout). It can be seen in Figure 5.11 that a 5 kW f-4.1, 1 atm plasma will remain stable until 53.0 kg/m^2s whereas a similar f-7.1 plasma only until 30.6 kg/m^2s. However this effect does not occur for 2.5 kW plasmas. At 2.5 kW, f-4.1 and f-7.1 plasmas become unstable at nearly identical mass fluxes of 16.6 and 16.5 kg/m^2s respectively. It was originally thought that the spot size of the focused beam had a great effect on the blowout mass flux. The spot size for an f-7.1 beam is smaller than that for an f-4.1 beam [22]. This means that an f-7.1 focal spot would have a higher power density than an f-4.1 focal spot, and consequently a higher blowout mass flux. Unfortunately this statement

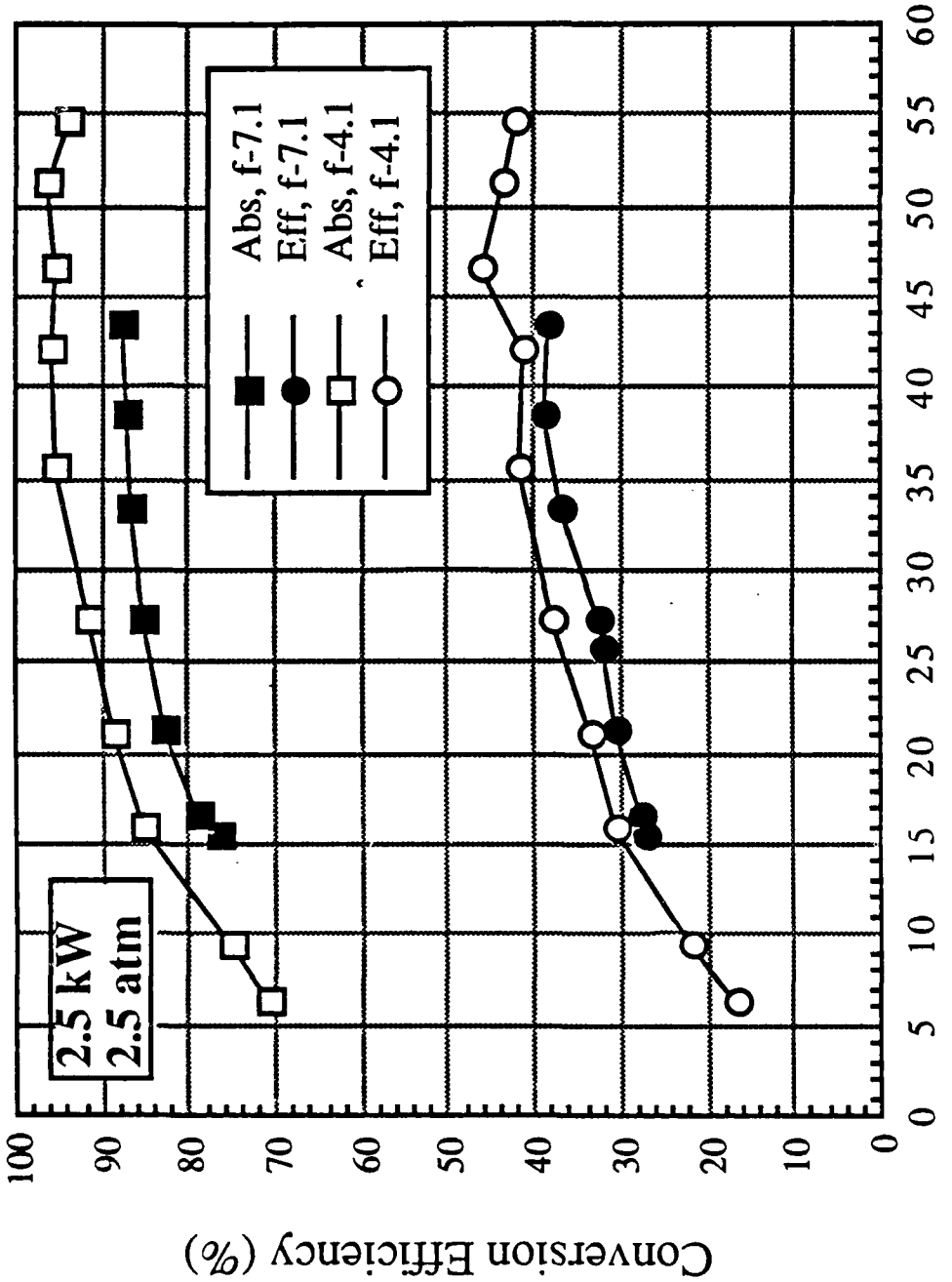

Figure 5.9 Comparison of global absorption and thermal efficiency for pure argon 2.5 kW, 2.5 atm. LSP's at f-4.1 and f-7.1 focusing geometries. Note that both absorptions and efficiencies are higher for the f-4.1 LSP's than for the f-7.1 LSP's.

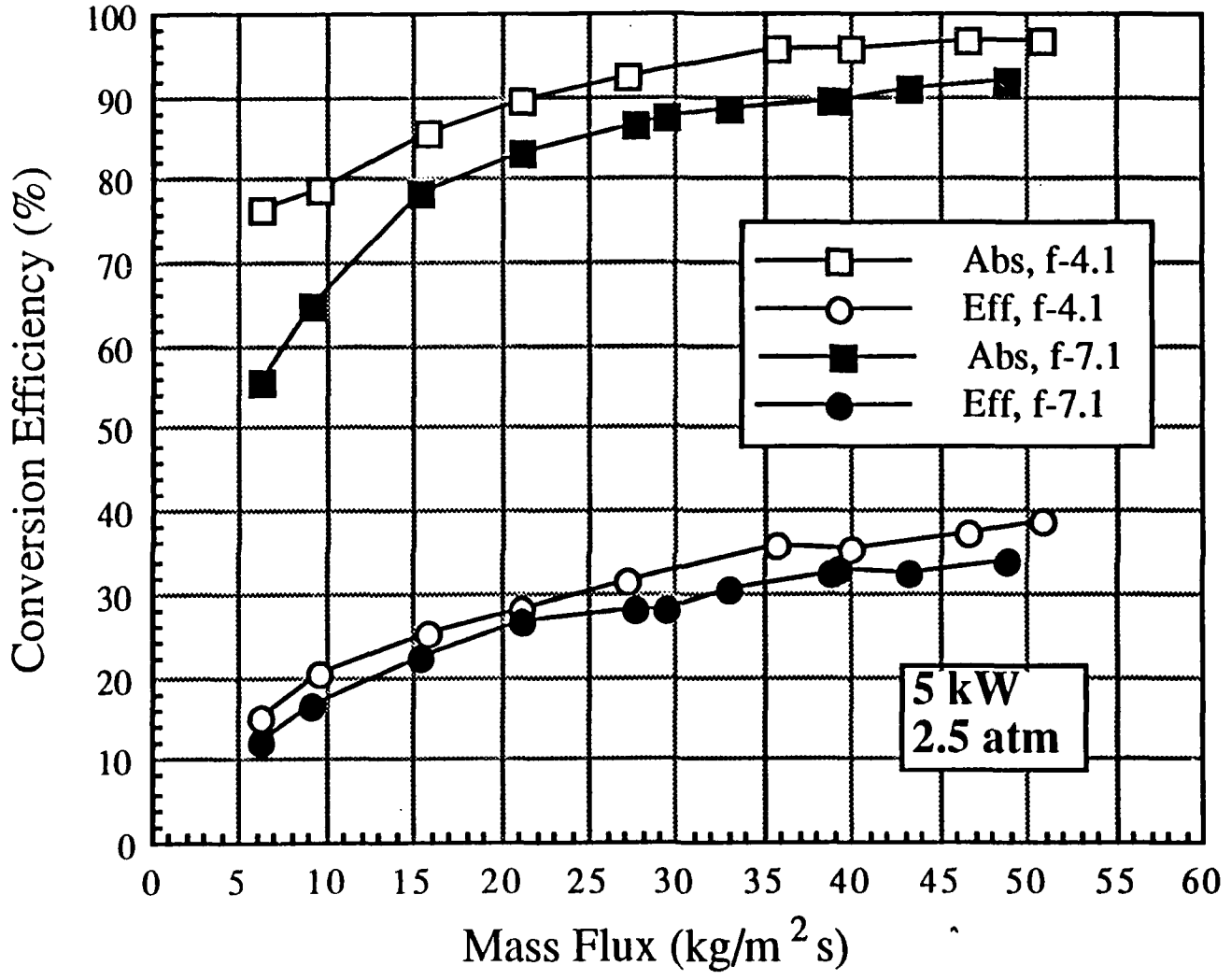

Figure 5.10 Comparison of global absorption and thermal efficiency for pure argon 5 kW, 2.5 atm. LSP's at f-4.1 and f-7.1 focusing geometries. Note that both absorptions and efficiencies are higher for the f-4.1 LSP's than for the f-7.1 LSP's.

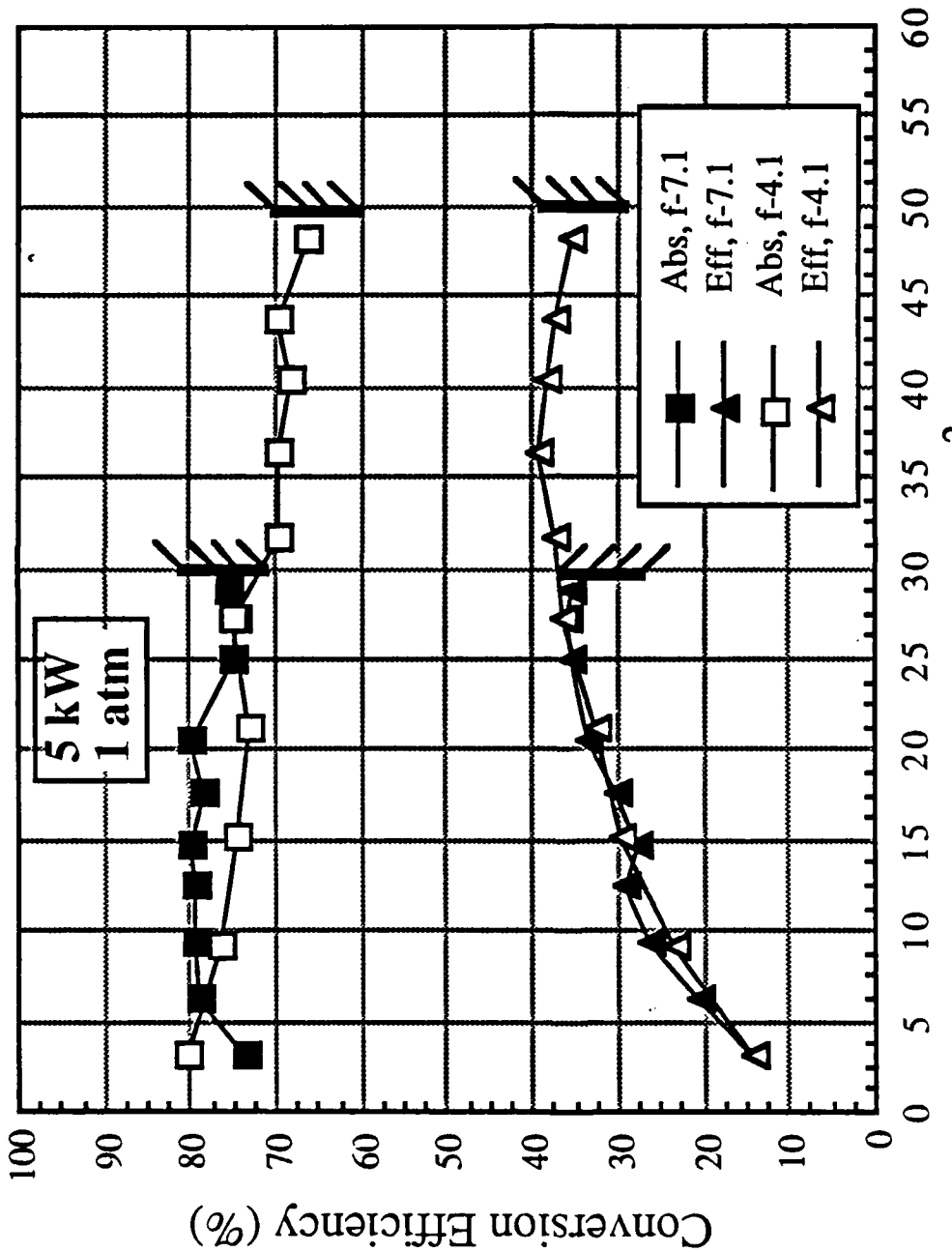

Figure 5.11 Comparison of global absorption and thermal efficiency for pure argon 5 kW, 1 atm. LSP's at f-4.1 and f-7.1 focusing geometries. Walls superimposed on figure denote LSP stability mass flux limits. Note the large difference in blowout mass flux for the two focusing geometries.

does not agree with observed blowout results. Therefore it can be concluded that spot size has a minor effect on blowout and that there is some other more influential factor to be considered.

The second factor may be the fact that the f-7.1 focusing geometry is more slender than the f-4.1 geometry and more closely resembles a parallel beam. It has already been seen that f-7.1 plasmas become unstable at 2.5 atmospheres pressure and low mass fluxes. Since the f-7.1 beam is more slender than the f-4.1 beam, f-7.1 plasmas would have a larger range of travel for small variations in power or mass flux. If plasmas at both geometries were near blowout and a small perturbation were to occur, the f-4.1 plasma would move a smaller distance to adjust than would the f-7.1 plasma. Since it has been observed that plasmas tend to oscillate (shift position upstream or downstream) due to small flow perturbations near the blowout mass flux, the smaller travel distance of the f-4.1 plasma would make it easier for the plasma to adjust and less likely to become unstable.

5.4. Mass Flux Effects

Mass flux (the product of density and velocity) is a key parameter involved in controlling a LSP's position relative to the beam focus. Consequently, mass flux is also a key parameter in determining LSP stability, global absorption, and thermal efficiency. Since mass flux was the parameter with the greatest degree of variation in this study, we have learned much about LSP behavior throughout the range of available mass fluxes.

In general regardless of laser input power, gas pressure, or beam focusing geometry, at low mass fluxes the LSP is far upstream in the beam and intercepts the beam in a low power density region and through a short length. As the mass flux is increased, the LSP moves downstream towards the focus and the global absorption increases. As the mass flux is increased further, the global absorption peaks as the LSP gets near the focus and intercepts a higher power density region of the beam through a longer length. Then as the mass flux approaches that required for blowout, the LSP wave front is at the focus and much of the plasma tail is actually not in the beam so the global absorption decreases. For the mass fluxes in this study, global absorption has been seen to decrease with mass flux at 1 atmosphere

pressure (as can be seen in Figure 5.3) because the mass flux is already beyond that required for peak absorption at 1 atmosphere. The dramatic effect of mass flux plasma position can be seen in the comparison of photographs in Figure 5.12.

The behavior of thermal efficiency with mass flux variation qualitatively resembles the global absorption behavior. At low mass fluxes the LSP has a low global absorption, and consequently also has a low thermal efficiency. As mass flux is increased, there is an increase in thermal efficiency despite the rise in LSP radiation losses due to higher global absorption. At these mass fluxes, the plasma could be described as a relatively short and hot plasma with high radiation losses. As the global absorption peaks the thermal efficiency will continue to increase. A further increase in mass flux causes the global absorption to decrease, but because of decreased LSP radiation losses the thermal efficiency continues to rise. Now the LSP could be described as a long cool plasma with low radiation losses. Finally, as the global absorption continues to decrease, the thermal efficiency peaks and then decreases until the LSP becomes unstable. This peak in thermal efficiency can be seen in the data of Figures 5.3, and 5.5 for 1 atmosphere plasmas and in Figure 5.7 for 2.5 atmosphere plasmas. The highest recorded thermal efficiency using pure argon was 46% for a 2.5 atmosphere, f-4.1, 2.5 kW plasma at approximately 47 kg/m^2s and can be seen plotted in Figures. 5.7 and 5.9. The general trends of global absorption and thermal efficiency versus mass flux are shown in Figure 5.13.

5.5. Helium/Argon Mixtures

In this section the effects of helium addition on plasma absorption of incident laser energy, plasma irradiation, and energy transferred to the gas flowing around and through the plasma will be discussed. A comparison of specific heat and electron number density of helium and argon is presented in Figure 5.14.

The results of experiments performed at a laser input power of 5kW, chamber pressure of 2.5 atmospheres, and f/4.1 beam geometry are presented in Figure 5.15. Data is shown for three different gas mixtures: pure argon, 33% helium by volume in argon, and 50% helium by volume in argon. Thermal efficiency ranges from 15.1% at low mole flux pure argon to a peak

Figure 5.12 Double exposure photographs of a 3.1 kg/m^{2}s, 7 kW, 1 atm., f-7.1 pure argon LSP (left) and a 32.2 kg/m^{2}s, 7 kW, 1 atm., f-7.1 pure argon LSP (right). The beam focusing geometry has been superimposed on the photographs for clarity and to show the position of the focus. Note that the 3.1 kg/m^{2}s LSP is much further upstream (lower in the tube) than the 32.2 kg/m^{2}s LSP.

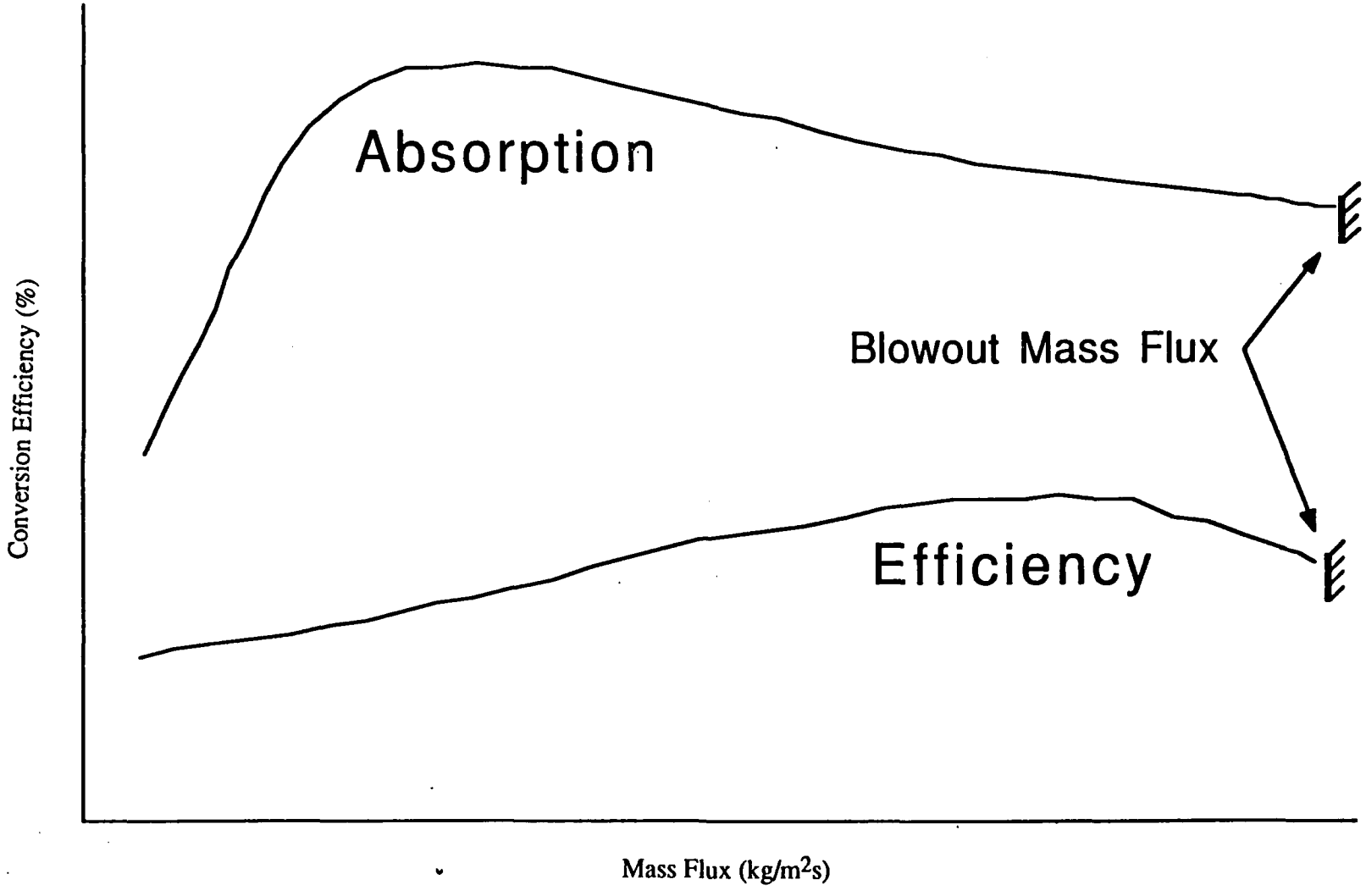

Figure 5.13 General trends of global absorption and thermal efficiency versus mass flux for a fixed input power and pressure.

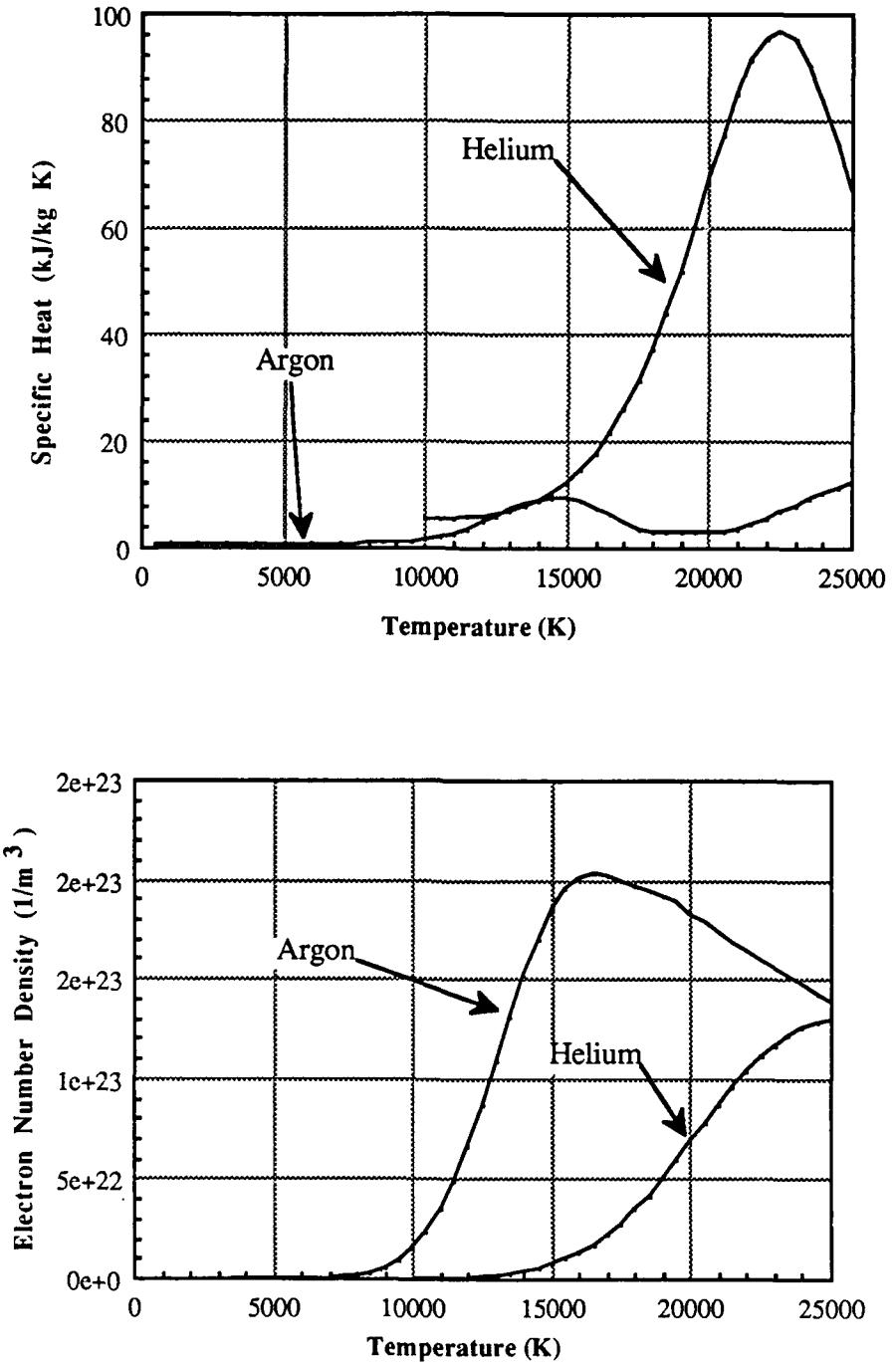

Figure 5.14 Specific heat and electron number density versus temperature for argon and helium.

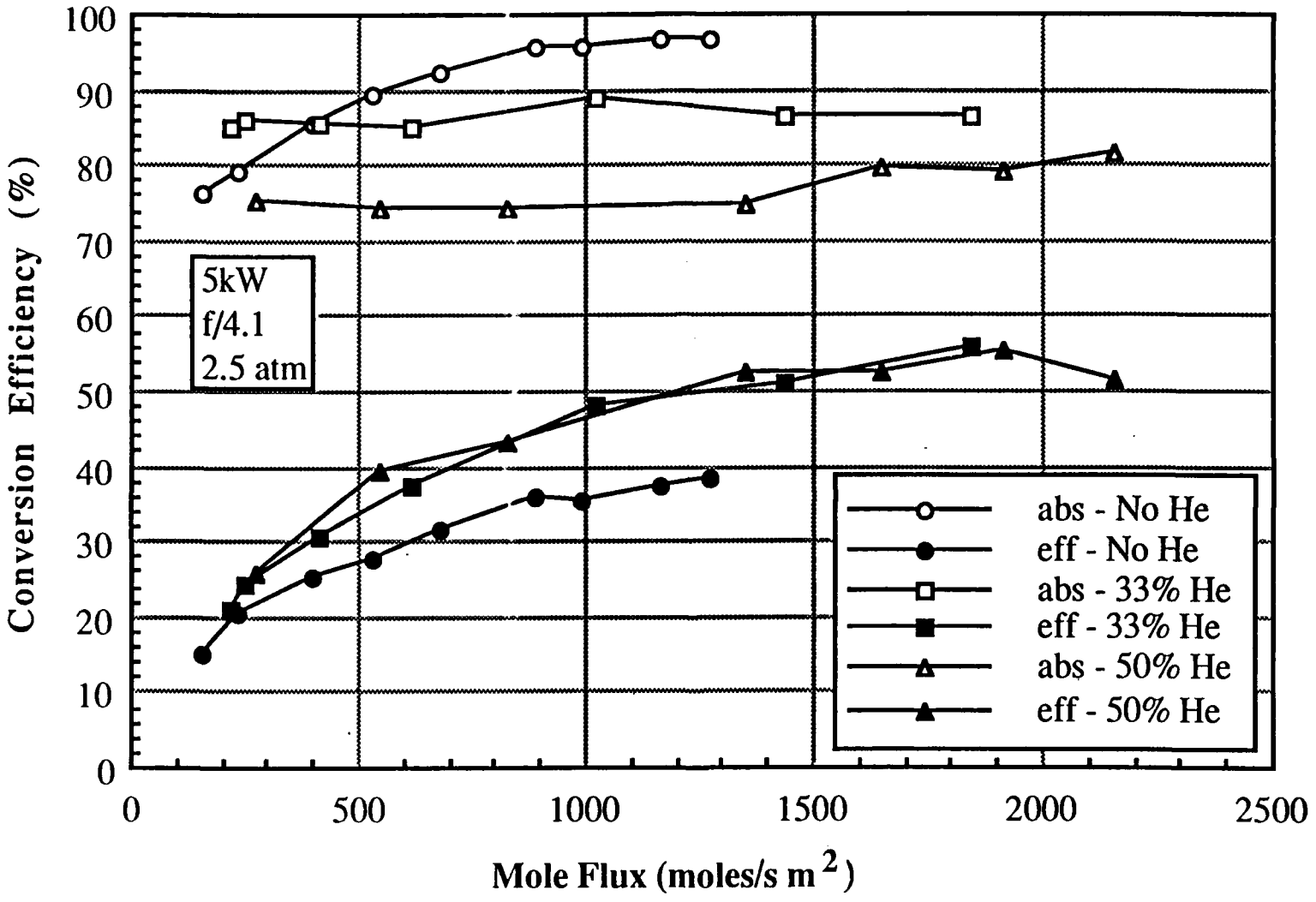

Figure 5.15 Comparison of global absorption and thermal efficiency for helium/argon mixture LSP's at 5 kW, 2.5 atmospheres and f/4.1 beam geometry. Results for pure argon, 33% helium by volume, and 50% helium by volume are presented.

value of 56.1% at a relatively high mole flux and 33% helium. The percentage of incident laser energy absorbed by the plasma is also shown in Figure 5.15. As can be seen from the graph nearly 98% of the incident laser energy is absorbed by plasmas formed in pure argon at mole fluxes greater than 800 moles/m^2s. The lowest levels of absorption, 75% for most of the mole fluxes covered in this study, occurred for plasmas produced in 50% helium mixtures.

Figure 5.16 is a comparison of 2.5kW, f/4, 2.5 atmosphere plasmas formed in pure argon and in a mixture of 33% helium. Thermal efficiency ranges from 16.3% at low mole flux and no helium, to 49.9% at a mole flux of 1015 moles/m^2s and 33% helium. Absorption ranges from 70% at low mole flux to over 90% at high mole fluxes.

Absorption trends in the data of Figures 5.15 and 5.16 indicate that the addition of helium to the argon flow decreases the amount of laser radiation absorbed within the plasma. Only at low mole fluxes do the helium/argon plasmas absorb more than pure argon plasmas. Also whereas pure argon plasma absorption increases with increasing mole flux until reaching over 95%, plasmas formed in helium/argon mixtures demonstrate a nearly constant absorption for the mole fluxes presented.

As stated earlier inverse bremsstrahlung (IB) absorption is the primary mechanism by which the plasmas involved in this study absorb incident laser radiation. Also recall that for IB absorption to occur free electrons must be present. Spectroscopic analysis confirms that due to its high ionization potential and relatively low plasma temperatures helium does not ionize significantly within plasmas sustained at the conditions presented here. Therefore helium does not contribute many free electrons which could be involved in IB absorption and the electron number density of the mixture is presumed to have decreased. Because helium and argon have such different degrees of ionization for the temperatures involved in this study an absorption coefficient is very difficult to calculate for these experiments.

It is important to point out that the IB absorption coefficient is directly proportional to the number density of free electrons within the gas. Absorption coefficient and mole flux determine where a plasma will stabilize in a focused beam. It is therefore necessary to examine

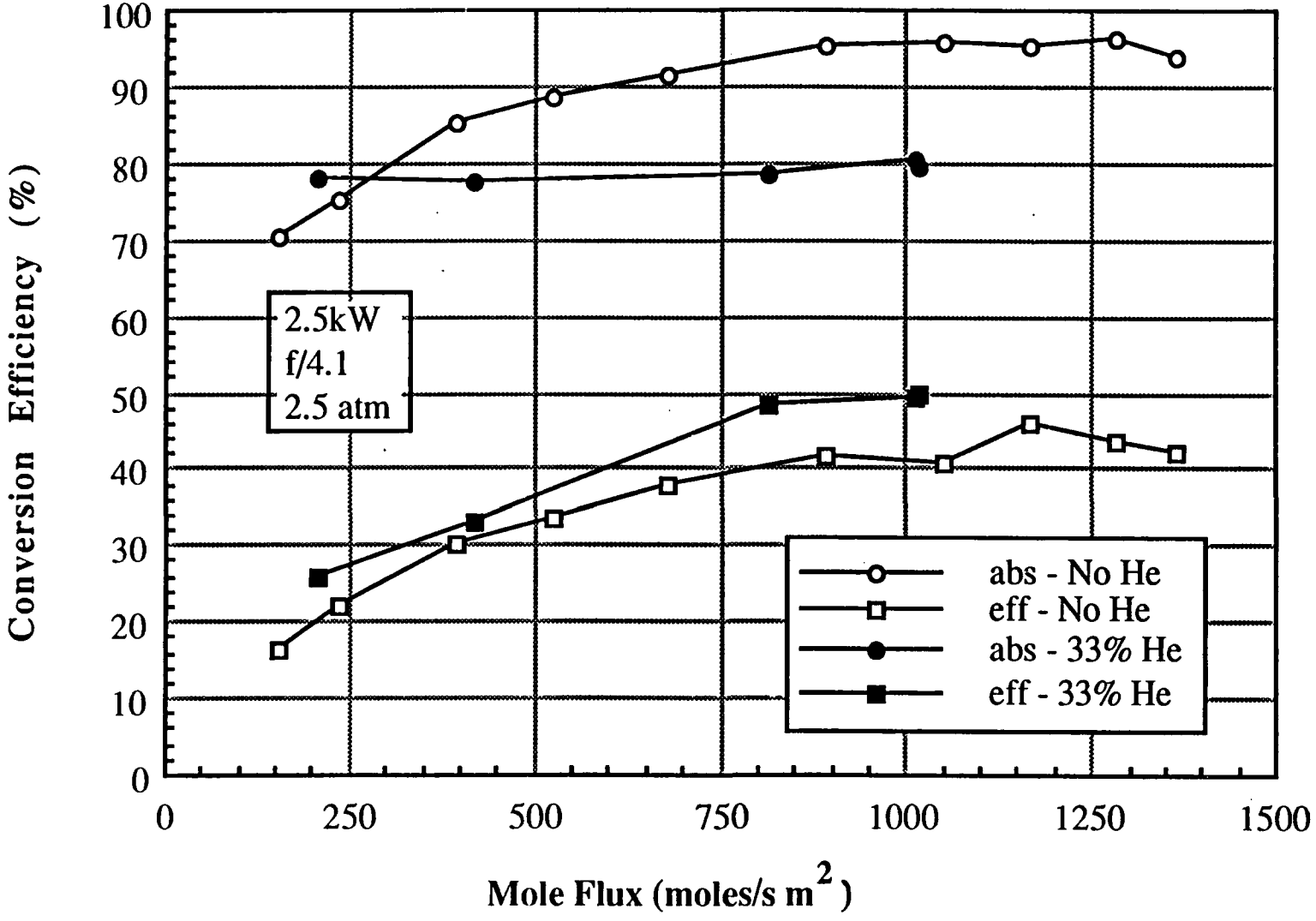

Figure 5.16 Comparison of global absorption and thermal efficiency for helium/argon mixture LSP's at 2.5 kW, 2.5 atmospheres and f/4.1 beam geometry. Results for pure argon and 33% helium by volume are presented.

the effect of helium addition on plasma position and consequently on absorption and thermal efficiency.

Consider a situation in which the total mole flux is fixed, then the addition of helium reduces the number of argon atoms per unit volume, thereby reducing the total number of argon atoms available for the contribution of free electrons to the gas. The reduction in electrons in turn lowers the absorption coefficient of the gas. Because of lower absorption coefficients one expects that plasmas sustained in helium/argon mixtures will stabilize in a region of greater laser intensity (i.e. closer to the laser focus) where more energy can be absorbed.

The effects on the plasma of changing the amount of helium in the gas mixture at a fixed mole flux is illustrated in Figure 5.17. The plasma shape and location were traced on paper placed over a 35mm filtered photograph. The tracing paper was then placed over a second photograph at the same location relative to several fixed points in the background as in the first photograph. The outline of the plasma on the second photograph was then traced over the outline of the previous plasma. Figure 5.17 confirms the theory of helium addition causing the plasma to stabilize closer to the focus as helium is added.

Note however, that at low mole fluxes the absorption of helium/argon plasmas is actually greater than that of pure argon. Low mole flux argon plasmas stabilize upstream of the focus at a location of relatively low laser intensity. Figure 5.17 indicates that plasmas sustained in low mole flux helium/argon mixtures stabilize much further downstream than pure argon corresponding to a region of greater laser intensity. By stabilizing in a region of much greater laser intensity helium/argon plasmas may overcome the reduction in electron number density, so that in fact helium/argon plasmas at low mole fluxes can absorb more than pure argon plasmas. At greater mole fluxes both pure argon plasmas and helium/argon plasmas stabilize near the focus and the difference in plasma location is not significant enough to overcome the lack of free electrons. Correspondingly plasma absorption for helium/argon mixtures at high mole fluxes is less than that for pure argon.

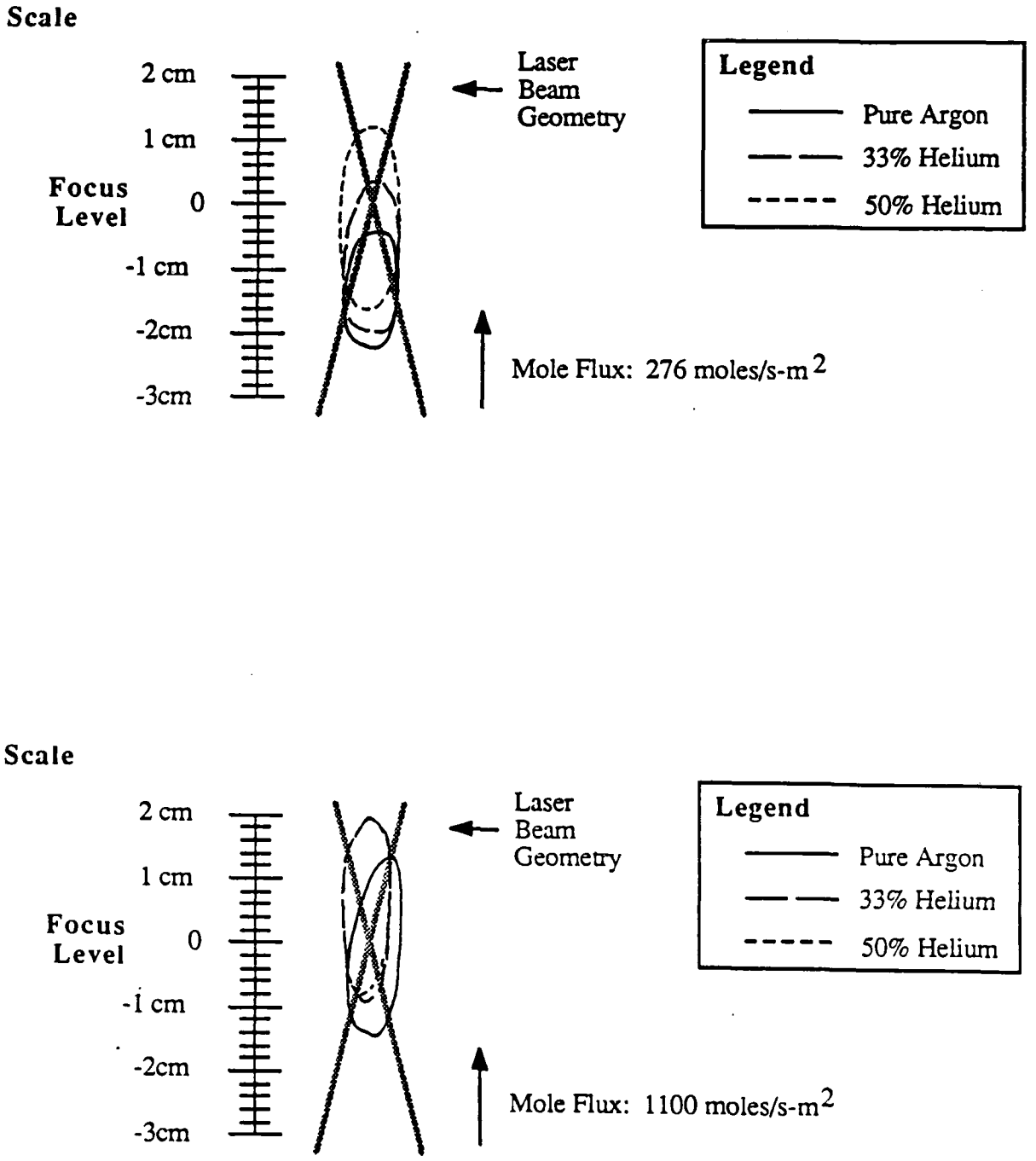

Figure 5.17 Effect of helium addition at fixed total mole flux on plasma position. Note that an increase in volume percentage of helium causes the plasma to stabilize closer to the beam focus.

Plasma radiative losses are also dependent upon electron number density. As stated in Oettinger [9] continuum radiation loss is found to be a function of number density and temperature. Spectroscopic analysis has shown that overall plasma temperatures at a given mole flux decrease with the addition of helium. From the argument above it has already been shown that electron number density decreases with the addition of helium to the flow. Together these two effects predict that the addition of helium should decrease plasma radiation losses. The data presented in Figures 5.15 and 5.16 confirm that this is indeed the case. The plasma radiative loss is represented in Figures 5.15 and 5.16 by the difference between the absorption and thermal efficiency curves (e.g. the sum of the energy retained by the gas and energy radiated to the surroundings equals the energy absorbed by the plasma). In fact the radiation losses by helium/argon plasmas are so low that the thermal efficiency of such plasmas is greater than pure argon plasmas even though their absorption is significantly less. Also note that radiation loss decreases with the amount of helium added.

The thermal efficiency of 33% helium/argon plasmas is significantly greater than that of pure argon plasmas as can be seen in the data of Figures 5.15 and 5.16. As can be seen in Figure 5.15 the addition of helium has little effect on thermal efficiency at low mole fluxes. However as mole flux increases so does the difference between the pure argon and 33% helium results. At a mole flux of nearly 1300 moles/m^2s the thermal efficiency increases from 38% for pure argon to 50% for a mixture of 33% helium. Greater fractions of helium however do not continue to increase thermal efficiency. The thermal efficiency results of 33% and 50% helium/argon plasmas do not differ greatly and are within experimental error. The maximum thermal efficiency reported is 56% at a mole flux of 1845 moles/m^2s and 33% helium gas mixture. This is a significant finding because the 50% thermal efficiency level has been viewed as the limit beyond which laser propulsion becomes feasible [4].

The increase in thermal efficiency reported in Figures 5.15 and 5.16 can be attributed to several factors. First is the reduced radiation loss argument discussed above. At a fixed absorption level reduction in radiation losses allows for an increase in energy transferred to the

gas. This effect is closely linked to the thermophysical properties of helium. The thermal conductivity of helium, like hydrogen, is an order of magnitude greater than that of argon. Thermal conductivity defines the rate of heat transfer within a material. Therefore heat diffuses much more rapidly in helium gas compared to argon gas. The specific heat of helium is also approximately ten times greater than that of argon. Thus a much larger amount of energy is transferred to helium for a small temperature increase whereas argon requires a larger temperature increase.

In addition the rate of elastic collisions between free electrons and helium atoms is much greater than for electrons and argon atoms. This is due to the Ramsauer effect associated with that argon atoms at the electrons energies dominant in the plasma (1-2 eV) [34]. This coupled with the much lower atomic weight of helium leads to more efficient energy transfer from the hot electrons and the cold helium atoms than may be occurring in pure argon plasmas.

The results also suggest the possibility of achieving a maximum thermal efficiency at a given mole flux by the correct gas mixture selection. Figure 5.18 shows the absorption and thermal efficiency of plasmas at a total mole flux of 829 moles/m^2s at different percentages of helium. Pure argon absorption is 95.5% and thermal efficiency 35.8%. The highest thermal efficiency is 47.8% at 33% helium with 88.7% absorption. The data presented in Figures 5.15 and 5.18 indicates that for plasmas in a mixture range from 30 to 50% the thermal efficiency is fairly constant while absorption decreases as helium increases.

These mixture plasma experiments were performed as a preliminary study into the results of using hydrogen as the operating gas. Even though helium did not ionize significantly in these experiments, and its absorption and emission characteristics differ from that of hydrogen it does possess thermodynamic propertie similar to hydrogen. The results of these experiments suggest that the high thermal conductivity and specific heat of hydrogen will aid in the production of high thermal efficiencies.

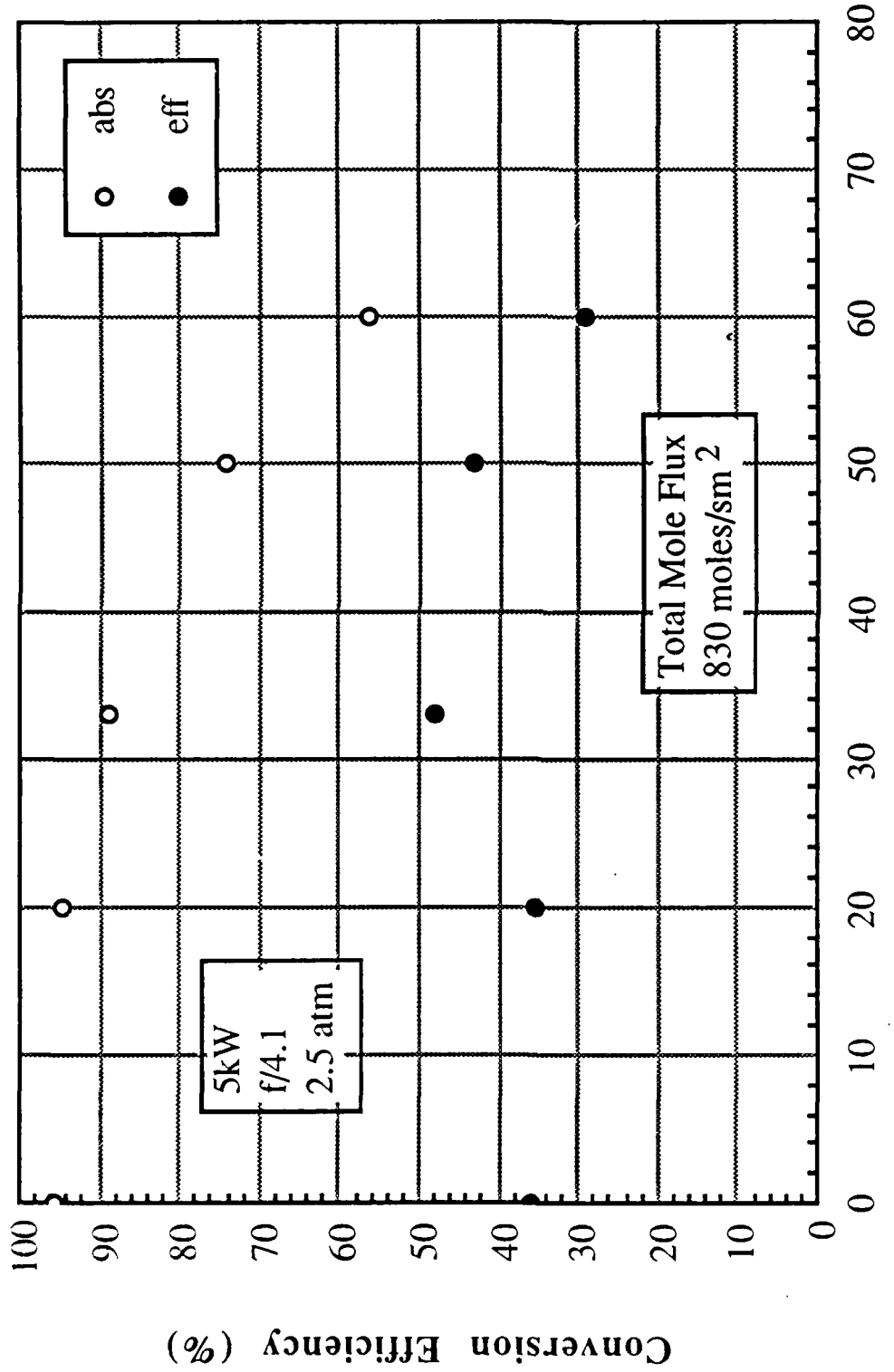

Figure 5.18 Global absorption and thermal efficiency for 5 kW, f/4.1, 2.5 atmosphere plasmas at a fixed mole rate of 830 moles/sm^2 and variable percentage of helium.

5.6. LSP Modeling Status

To complement the experimental work, numerical modeling has also been pursued at the University of Illinois at Urbana-Champaign(UIUC). The Glumb-Krier Quasi 2-D model had some success in qualitatively predicting the effects of varying mass flux and f-number on absorption and energy conversion efficiency in argon plasmas [18]. However, the assumptions of zero radial velocity and constant axial mass flux (ρu) do not allow for the quantitative accuracy necessary for direct comparison to experiment. Furthermore, a fully 2-D model created at the University of Tennessee Space Institute (UTSI) proved that radial momentum transport is too significant in determining plasma size and position to neglect [35].

For the above reasons, it was decided that a full 2-D model, which maintains the highest accuracy available in the thermodynamic and thermal energy transport properties, must be developed at the UIUC. This new model would entail simultaneous solution of equations of state, mass conservation, u and v momentum conservation, and energy conservation. The TEACH code, based on the SIMPLE algorithm as described in Patankar, is being used to model the LSP conditions [36].

The assumptions upon which the solutions are based are steady state, axisymmetric, laminar flow under conditions of local thermodynamic equilibrium (LTE). The laser energy input is treated as a source in the energy equation. The laser energy distribution is modeled after a converging annular beam with a gaussian intensity distribution across its ring. Both spot size and f-number may be varied. The actual geometry and optics is based on laser burns from the experimental facility. The absorption is calculated by invoking Beer's Law along the laser path.

The radiation from the plasma is treated by separating it into optically thin and thick contributions to radiation transport. The optically thin radiation refers to the continuum free-free and free-bound emission, and radiation loss due to bound-bound line emission which is not reabsorbed by the plasma and may be considered lost to our thermal energy conversion

process. This portion of the overall radiation loss is treated as an energy sink in the energy equation.

The optically thick radiation refers to the radiated energy which is reabsorbed and thereby retained by the plasma. This contribution acts as an induced radiative conductivity which is added to the thermal conductivity. This contribution to conductivity is in fact the dominant diffusion transport mechanism of energy in the plasma temperature regions above 10000 K.

The buoyancy term in the momentum equations must also be considered. Since in the laboratory the plasma is sustained in a vertical apparatus, the buoyancy term (ρg) is applied in the u-momentum equation describing axial momentum in a vertical direction. Dr. San-Mou Jeng at UTSI has stated that inclusion of the buoyancy term in the momentum equation made negligible difference on the overall flow and energy conversion characteristics of the plasma [37]. To verify this a calculation of the ratio Gr/Re^2, i.e. the measure of the buoyancy versus viscous effects, can be made for the conditions encountered in the plasma. The following calculation is for a 5kW plasma being convected by .5 m/s at the inlet.

Based on a pipe diameter of D = .04 m, and properties (density, viscosity) at 300 and 15000 K:

$$Gr_x = \frac{g x^3 \left(\frac{\rho_\infty}{\rho} - 1 \right)}{\nu^2}$$

$$Re_x = \frac{ux}{\nu} \qquad \text{(u from 2D code at ~ 15000K)}$$

So $$\frac{Gr}{Re^2} = \frac{3609}{3280^2} = 3.4\text{e-}04 \ll 1$$

<u>Conclusion:</u> Free convection is negligible so buoyancy term in the u-momentum equation has only a small effect on the flowfield.

Furthermore, the code was run with and without the buoyancy term as a check and the effect of buoyancy did prove negligible. For completeness, this term is kept for the numerical solution.

The key to accuracy in LSP modeling is the physical property data. The expressions upon which absorption coefficients and radiation losses are based are restricted to conditions of LTE. The results under LTE mean that the temperatures of the heavier particles within the plasma (atoms,ions) are assumed to be the same as the electron temperatures. The validity of the LTE assumption is discussed in Chapter Two. The property data implemented is presented in Table 5.1.

Table 5.1. Argon Property Data Used in Numerical Model

Property	Temperature Range	Reference Source
Specific Heat	≤ 6500 K	Howell, J.R., and Buckius, R.O. [38]
	> 6500 K	Drellishak et. al. [26]
Enthalpy	≤ 6500 K	Equal to specific heat from Howell and Buckius multiplied by T
	> 6500 K	Drellishak et. al.
Electron Number Density	≤ 20000 K	Dresvin, S.V. [25]
	> 20000 K	Extrapolation from Dresvin
Continuum Radiation Loss	300 - 25000 K	Oettinger, P.E., and Bershader, D. [9]
Line Radiation Loss	300 - 25000 K	Kozlov et. al. [10]
Absorption Coefficient	300 - 25000 K	Wheeler, C.B., and Fielding, S.J. [7] (Correction for Argon from Stallcop [8])
Thermal Conductivity	300 - 5000 K	Vargaftik [39]
	5000 - 7000 K	Sergienko [40]
	≥ 7000 K	Bues [41]
Viscosity	300 - 1300 K	Vargaftik
	1300 - 3000 K	Linear interpolation
	≥ 3000 K	DeVoto [42]
Density	< 7000 K	Ideal Gas Law
	≥ 7000 K	Drellishak et. al.

Preliminary calculations for a 5kW laser power source of f/7 beam geometry have verified the important role of radial momentum transfer to the determination of plasma size, shape, and position. These have a direct effect on energy conversion efficiency since plasma geometry with respect to laser intensity determines how much energy may be absorbed.

Figure 5.19 is a comparison between the model and experiment results for an argon plasma at one atmosphere sustained by an f/7 and 5kW laser beam. The absorption calculated by the code is slightly higher, as is the thermal efficiency, than what is observed in the experiments. However, the trends exhibited by both the absorption and efficiency is well represented. The difference in magnitude which does exist may be due to the code's adiabatic wall boundary condition. Therefore the code does not account for any energy losses to the walls. The code's wall boundary condition could be changed to more accurately reflect the experiment's heated wall, but since this is a somewhat transient phenomena in the lab depending on how long the plasma has been sustained, the adiabatic wall assumption will be kept initially.

At the UIUC, the goals of the modeling work are to scale the physical processes observed in the experimental facility to laser power and flow rates unattainable in the lab. A comparison will also be made between the laminar cases run with the new code with those run previously by the quasi 2-D code. Laminar cases will be run for both argon and hydrogen. Good agreement between experiment and modelling for argon plasmas will establish confidence in applying the code to the calculation of hydrogen plasma behavior. This will prove valuable upon the initiation of work on hydrogen LSPs at the UIUC.

In the future, to approach the latest mass flux conditions tested in the experimental facility, turbulence must be included in the code. The experimental work has shown that peak efficiencies are occurring near plasma blowout and therefore determination of the blowout velocity is of great importance. The mass fluxes required for blowout necessitate running at high mass fluxes and solution of turbulent transport equations.

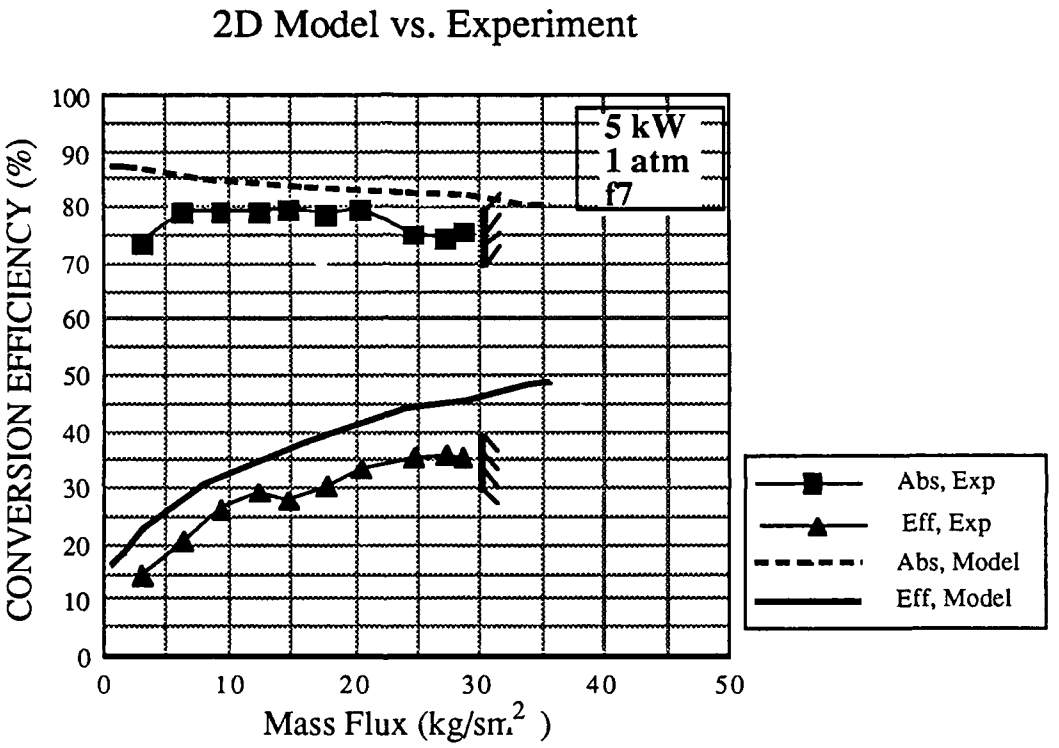

Figure 5.19. Comparing absorption and efficiency between experimental data and modeling results for an f7, 5kW, 1 atmosphere Argon LSP.

Another important issue is raised by the assumption of local thermodynamic equilibrium. Future experimental work at the UIUC, as discussed in Chapter 2, intends to determine whether or not the plasma is in LTE. If it is determined that we are not in LTE, the logical step is to pursue a two-temperature model. The most difficult issue to address again would be accurate property data, this time for a non-LTE environment.

Chapter 6. Conclusions and Recommendations

The behavior of LSP's with variations of input parameters has been described and explained for pure argon plasmas and helium/argon plasmas. In this chapter important trends will be summarized and optimization of LSP thermal efficiency will be briefly discussed.

6.1. Summary of Results

Increases in either power or pressure cause an upstream shift in LSP position and a corresponding increase in LSP blowout mass flux. An increase in power will cause an increase in global absorption and a decrease in thermal efficiency for a given mass flux. An increase in pressure will cause a decrease in thermal efficiency for a given mass flux, however, it was found that the maximum global absorptions and thermal efficiencies that can be achieved increased with power and pressure.

The major effect of f-number variation was in the area of LSP stability. The more slender f-7.1 beam geometry produced plasmas that were less able to withstand small flow perturbations when the plasma was very near the focus which resulted in the f-7.1 plasmas becoming unstable at lower mass fluxes than f-4.1 plasmas. Focal spot size was found to be a minor consideration in these experiments although its effect could have been substantial if the difference in f-numbers used had been larger.

Mass flux was found to be the key parameter in controlling and optimizing plasma behavior. Global absorption was seen to decrease with mass flux at 1 atmosphere. Global absorption at 2.5 atmospheres increased with mass flux and then levelled off as the plasma wave front approached the beam focus. Thermal efficiency was found to increase with mass flux for both the 1 atmosphere and 2.5 atmosphere cases, and was then found to peak and decline just before blowout.

Addition of helium was found to cause the plasma to stabilize closer to the laser focus. At low mole fluxes mixture plasmas had a higher global absorption than pure argon plasmas, but as mole flux was increased pure argon plasmas had the higher global absorption. Even with a

lower global absorption, mixture plasmas resulted in higher thermal efficiencies than pure argon plasmas due to reduced radiation losses.

Other important findings include values of global absorption of 97% and thermal efficiency of 46% which are higher than ever previously recorded in pure argon. Within the bounds of uncertainty this value (97%) could represent complete absorption of input power. The 46% value for thermal efficiency is near to the generally accepted concept feasibility threshold of 50%. The maximum measured values of global absorption and thermal efficiency at 1 atmosphere pressure were 80% for a 7 kW, f-7.1 plasma and 39% for a 5 kW, f-4.1 plasma respectively. The value of thermal efficiency of 56.1% recorded for a helium/argon mixture is the highest value yet recorded for thermal efficiency in any gas. We hope that when pure hydrogen gas is used that the high thermal conductivity and specific heat of hydrogen will result in even higher thermal efficiencies.

6.2. Optimization of LSP Thermal Efficiency

The complex interaction of the control parameters in this study make it apparent that there may be several ways to optimize LSP thermal efficiency. Other parameters that were fixed for this study and would probably be fixed in an actual thruster are the laser wavelength and choice of propellant gas. The propellant of choice in an actual thruster would be hydrogen. Since it has been seen that maximum achievable thermal efficiency increases with input power, the thruster would most likely be operated at the maximum power output of the source laser. Thus, referring back to equation (1.4), it can be seen that operating at maximum available power will produce not only the highest thermal efficiency but also the highest thrust and specific impulse. Since there would be no reason to vary the beam focusing geometry in an actual thruster, and to do so would add extra weight and design complications to the vehicle, it can be assumed that the focusing geometry would be fixed. Therefore in application the only two variable parameters remaining would be gas pressure and mass flux (or mole flux).

The experiments conducted at elevated pressure in this work used a valve downstream of the plasma chamber. Mass flux through the plasma chamber and the pressure within the

plasma chamber were thus separately controllable. Mass flux in an actual thruster would be a function of throat area, A^*, throat stagnation temperature, T_o, and chamber stagnation pressure, P_o. Since the Mach number of the throat would be unity, mass flux would be determined by the following relation:

$$\frac{\dot{m}}{A^*} = \left(\frac{\gamma}{RT_o}\right)^{\frac{1}{2}} \left(1+\frac{\gamma-1}{2}\right)^{\frac{-(1+\gamma)}{2(\gamma-1)}} P_o \qquad (6.1)$$

The left side of (6.1) is the mass flux (kg/sec m^2) and the right side is essentially a constant multiplying P_o, since T_o will likely be determined by the material limits of the thruster. Therefore optimization of thruster thermal efficiency would involve selection of the optimum combination of stagnation pressure and corresponding mass flux. The size of the throat may have to be adjusted somewhat in this process to get an optimum combination. Discussions of optimization of thruster performance can be found in detail in Reference 2, including sample case thruster designs.

6.3. Recommendations For Facility Improvement

The three inch gate valve used to control chamber pressure has no effect on chamber pressure until the valve gate is almost closed. Then a slight change in gate position causes a large change in chamber pressure, making it difficult to set the desired pressure. In addition, if the gas flow is turned off and then turned back on, the gate position will usually have to be reset to regain the desired chamber pressure. To facilitate more accurate and easier chamber pressure control, this three inch gate valve should be replaced with a smaller, automatically controlled valve for future high pressure experiments.

Another improvement (which has been implemented since the data for this work was acquired) is to use all ZnSe optics and no longer use NaCl components. Since the ZnSe optics are much more durable and easier to keep clean than NaCl, this improvement will save money lost to breakage of NaCl windows and damage to NaCl lenses even though the cost of ZnSe is

much greater than NaCl. To date no ZnSe component has been damaged other than minor scratches.

As mentioned earlier hydrogen is the propellent gas of choice for laser propulsion systems because of its potential for providing high specific impulse rocket thrust.

Because of the wide flammability limits for hydrogen/air mixtures the use of hydrogen in laser-sustained plasma experiments requires the addition of several safety features to the existing UIUC laboratory facility. Below is a brief description of several systems planned for the laboratory upgrade.

The most important addition to the laboratory is the equipment needed for the safe ventilation of the hydrogen used during experiments. Major concern is directed at preventing the hydrogen form drifting near university structures. Therefore the hydrogen will be exhausted to a level above the top of the building. This will involve a stainless steel pipe running from the test stand to the top of the laboratory roof.

Another important component is the ventilation of laboratory air near the experimental test stand. Currently planned is a five foot square fume hood directly above the plasma chamber. Connected to the hood will be a sparkless ventilation fan capable of exhausting 1000 cubic feet of air per minute. It will be standard operating procedure during experimental runs to keep the chamber pressure slightly above atmospheric conditions to ensure that no oxygen from the laboratory enters the chamber. The hood and fan will provide proper ventilation should hydrogen leak out of the chamber during operation.

Also to be installed in the laboratory are several detectors to monitor the level of hydrogen gas within the laboratory and gas storage area. These detectors will be connected to a central control panel located in the experiment control room. In the event of any detector being triggered the control panel will automatically shut off the hydrogen supply system.

The gas supply system will also be modified so the hydrogen supply can be remotely shut off if the gas system pressure drops below a preset level. The purpose of the pressure alarm set point is to insure that no room air seeps into the chamber, allowing only experimental gas to

leak out. Several additional pressure transducers will be placed throughout the gas network so the pressure of the entire system can be monitored.

An inert gas supply is also required in addition to the hydrogen supply. The inert gas will be used to purge the system of any oxygen before and after each experimental run in which hydrogen is used. A microprocessor controller will be used to control the chamber pressure during the transitions between purge and hydrogen gases to maintain the gas pressure at a safe level.

Fortunately the Fluke Model 2400B data acquisition and instrument controller computer purchased for this project several years ago is a powerful and diverse machine. By slightly modifying the computer code currently in use with the Fluke it will be able to operate several of the safety systems automatically. For example the Fluke will be able to monitor gas pressure and shut off the hydrogen supply if any of the pressures drop below a preset value. It will also be able to automatically shut off the laser in case of an emergency.

6.4. Future Work

Although argon LSP performance trends have been characterized fairly well by this and previous works, several new approaches exist that need to be researched to fully determine the future of LSP technology.

6.4.1. Two Stream Mixing

All the data presented in this work is for plasmas sustained in a single stream of argon accelerated with a quartz tube. This technique has been shown to produce almost complete absorption of the input laser power for certain conditions. Since one of the goals of this research is to optimize the thermal efficiency of LSP's, the next logical step would be to modify the existing flow pattern around the plasma to improve thermal mixing. In order to implement this a second stream of gas could be forced across the primary stream using a dual inlet system as shown in Figure 6.1. A separate flowmeter would be used to control the gas flow rates through each of the streams. In addition the actual position of the plasma could be varied from completely upstream of the second stream to the mixing region. Therefore, the

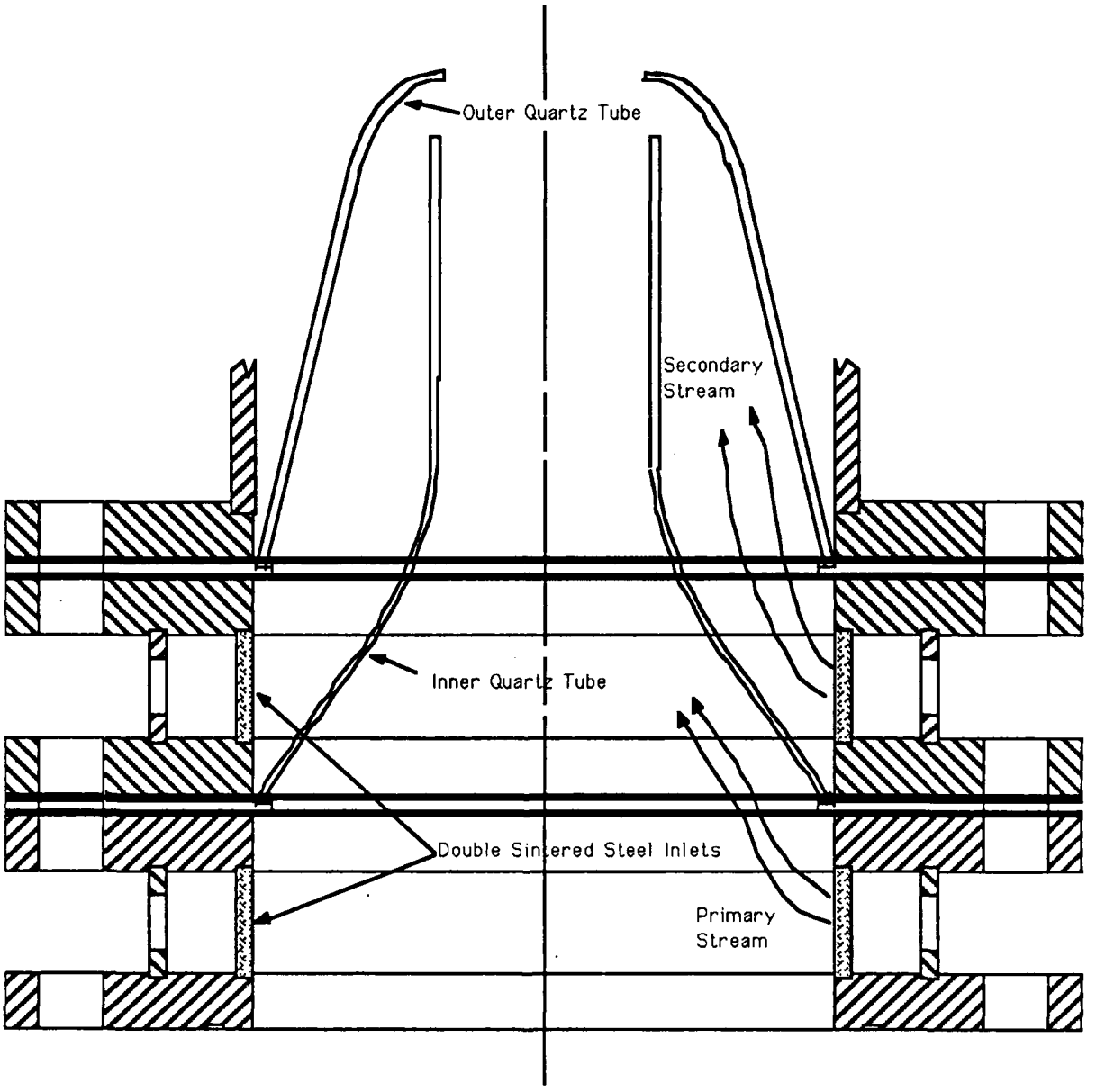

Figure 6.1 Schematic of dual inlet system to be used for two stream mixing experiments.

ratio of primary stream mass flux to secondary stream mass flux and the plasma position relative to the mixing region would be introduced as two new parameters to be optimized.

6.4.2. Hydrogen Experiments

Experiments conducted using hydrogen are the natural extension to the argon and argon/helium mixture experiments, and will determine whether laser thrusters can be made feasible. However, due to the highly explosive nature of hydrogen, special safety precautions must be taken in the laboratory to prevent accidents. A hydrogen safety system including exhaust hoods and hydrogen detectors has been designed by Scott Schwartz and is described in section 6.3.

6.4.3. Dual Plasmas

In an effort to reduce radiation losses from the plasma to the chamber walls, McMillin and co-workers first conducted experiments using two plasmas side by side [19, 20]. It is believed that two plasmas each with a given input power should have a higher thermal efficiency than a single plasma at the given input power. In addition the optimum mass flux for dual plasmas with a given total input power may be different than the optimum mass flux for a single plasma at half the given power. Dual plasma experiments will be conducted to compare the behavior of dual plasmas at a given total power (7 kW for example) with the behavior of single plasmas at the same power (7 kW) and single plasmas at the power of each of the dual plasmas (3.5 kW). In an effort to fully characterize dual plasma behavior, experiments will be conducted using dual plasmas with a variable separation distance. The technique for creating dual plasmas has not changed from the original technique [19, 20], but modifications have been made by Scott Schwartz to allow the plasma separation distance to be easily adjustable. Figure 6.2 is a schematic of the dual plasma split mirror apparatus. Experiments using dual plasmas could be conducted using argon or hydrogen and using a two stream mixing scheme. If the results obtained from dual plasmas appears promising, the idea could be extended to quad plasmas (by splitting the second turning mirror perpendicular to the third turning mirror)

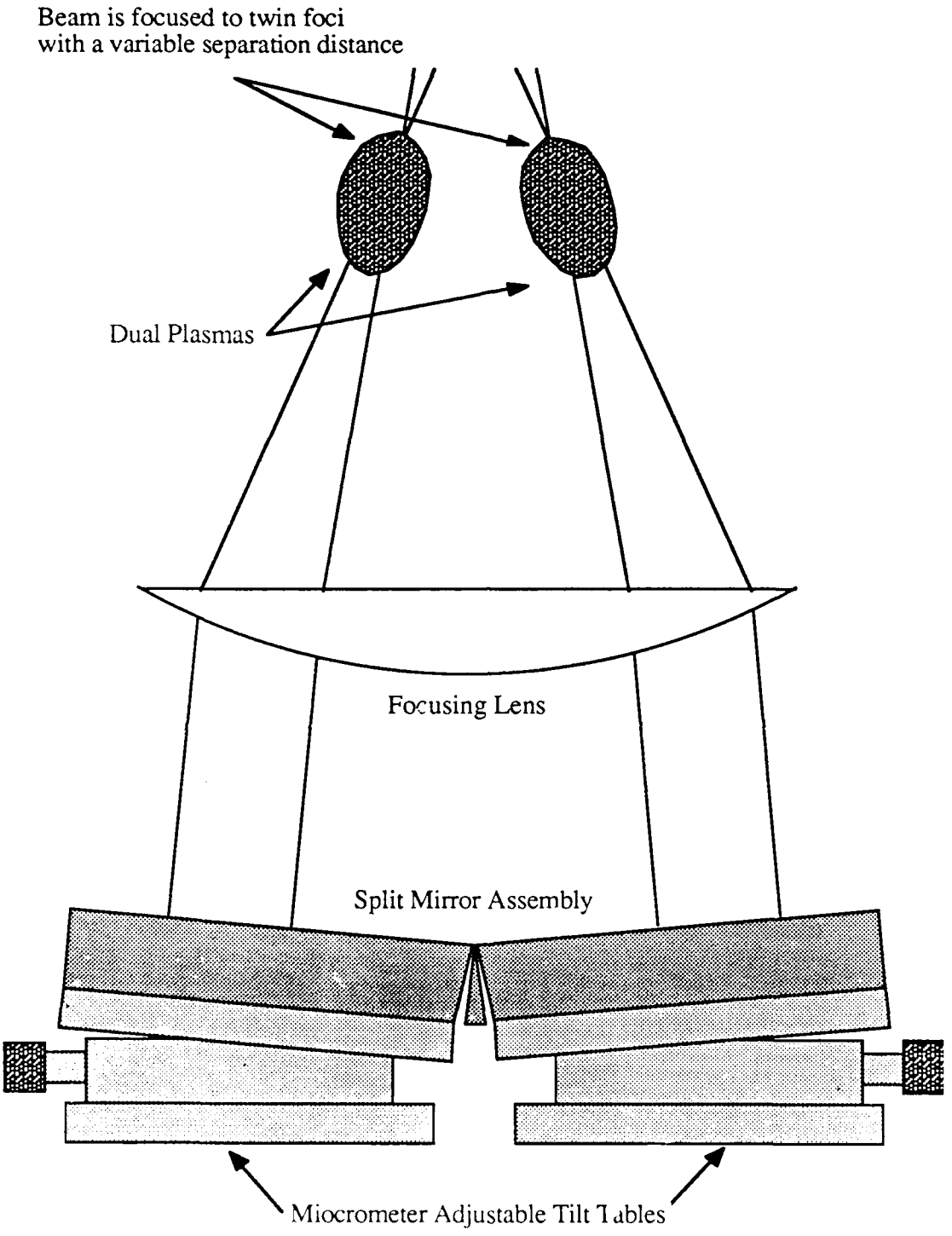

Figure 6.2 Schematic of dual plasma split mirror apparatus.

or possibly even ring plasmas (by use of an axicon lens to focus the annular beam to a ring).

6.4.4. Rayleigh Scattering Diagnostics

As mentioned in Chapter 2, there is a need for highly accurate plasma exhaust gas temperature measurements, and Rayleigh scattering thermometry appears to be a promising and relatively simple approach to the problem. Relative gas density can be gauged from the intensity of the Rayleigh scattering signal from different points in the flowfield. By measuring the Rayleigh scattered intensity from the flowfield at a known density (temperature), the absolute temperature in subsequent flowfields can be calculated from the ratio of scattered intensities [30].

The lower limit of the detection system dictates the maximum temperature which can be measured with this technique. This is because density decreases with temperature and hence the scattering signal is decreased. It is therefore important to produce as strong a signal as possible. Differential Rayleigh scattering cross section is inversely proportional to the wavelength of the incident radiation, so the eximer laser (ultraviolet output at 308 nm) currently available should provide an excellent source.

Initial experiments will be carried out us ng the OMA system described in Chapter 3. The intensity of the Rayleigh scattering line can be measured across the radial dimension of the flowfield, providing enough temperature information for efficiency calculations. This procedure takes advantage of a tightly focused beam (high intensity), and our present familiarity with the OMA detection system. Should this system prove successful, the technique will be advanced to two dimensional measurements. This will require focusing the beam into a planar sheet, and using optical filters rather than a monochromator for wavelength resolution. Beam intensity and thus scattered intensity will be decreased, but if such an experimental procedure can be implemented, complete instantaneous mappings of the downstream flowfield will be the benefit.

6.4.5. Plasma Core Diagnostics / LTE Studies

The need for the determination of the equilibrium status of a laser sustained plasma cannot be overemphasized. The progress toward this determination will be a major focus of the experimental work in the future. The measurement of electron number density, and independent calculations of electron temperature are realistic goals for this investigation. The direct measurement of heavy particle temperature would be a major breakthrough, and the optimisim for this undertaking is not unfounded.

References

1. Glumb, R.J., Experimental and Theoretical Studies of Laser-Sustained Argon Plasmas for Application to Laser-Supported Rocket Propulsion, Ph.D. Thesis, Department of Mechanical and Industrial Engineering, University of Illinois at Urbana-Champaign, June 1986.

2. Glumb, R.J., and Krier, H., "Continuous-Wave (CW) Thermal Laser Rocket Propulsion: Designing an Operational Thruster," Final Technical Report, Contract NAS 3-25271, Combustion Sciences Inc., July 1988.

3. Sutton, G.P., Rocket Propulsion Elements, Fifth Edition, John Wiley & Sons, Inc., 1986.

4. Glumb, R.J., and Krier, H., "Concepts and Status of Laser-Supported Rocket Propulsion," Journal of Spacecraft and Rockets, Vol. 21, No. 1, pp.70-79, January-February 1984.

5. Caveny, L.H., Ed., Orbit-Raising and Maneuvering Propulsion: Research Status and Needs, AIAA Progress in Astronautics and Aeronautics, Vol. 89, 1984.

6. Rockstroh, T.J., The Role of the Plasma During Laser-Gas and Laser-Metal Interactions, Ph.D. Thesis, Department of Mechanical and Industrial Engineering, University of Illinois at Urbana-Champaign, October 1986.

7. Wheeler, C.B., and Fielding, S.J., "Absorption of Infrared Radiation as a General Technique for Determination of Plasma Temperature," Plasma Physics, Vol. 12, pp. 551-564, 1970.

8. Stallcop, J.R., "Absorption Coefficients of a Hydrogen Plasma for Laser Radiation," Journal of Plasma Physics, Vol. 11, pp. 111-129, 1974.

9. Oettinger, P.E., and Bershader, D., "A Unified Treatment of the Relaxation Phenomenon in Radiating Argon Plasma Flows," AIAA Journal, Vol. 5, pp. 1625-1632, September 1967.

10. Kozlov, G.I., Kuznetsov, V.A., and Masyukov, V.A., "Radiative Losses by Argon Plasma and the Emissive Model of a Continuous Optical Discharge," Soviet Physics JETP, Vol. 39, pp. 463-468, September 1974.

11. Fowler, M.C., and Smith, D.C., "Ignition and Maintenance of Subsonic Plasma Waves in Air by CW CO_2 Laser Radiation," Journal of Applied Physics, Vol. 46, pp. 138-150, January 1975.

12. Van Zandt, D.M., McCay, T.D., and Eskridge, R.H., "An Experimental Study of Laser Supported Hydrogen Plasmas," AIAA Paper No. 84-1572, June 1984.

13. Welle, R., Keefer, D., and Peters, C., "Energy Conversion Efficiency in High-Flow Laser-Sustained Argon Plasmas," AIAA Paper No. 86-1077, May 1986.

14. Keefer, D., Welle, R , Peters, C., "Power Absorption in Laser-Sustained Argon Plasmas," AIAA Journal, Vol. 24, No. 10, pp. 1663-1669, October 1986.

15. Jeng, S.M., and Keefer, D., "Influence of Laser Beam Geometry and Wavelength on Laser-Sustained Plasmas,"AIAA Paper No. 87-1409, June 1987.

16. Mazumder, J., Rockstroh, T.J., and Krier, H. "Spectroscopic Studies of Plasmas During CW Laser Gas Heating in Flowing Argon," accepted by the Journal of Applied Physics, 1987.

17. Krier, H., Mazumder, J., Rockstroh, T.J., Bender, T.D., and Glumb, R.J., "Studies of Continuous Wave Laser Gas Heating by Sustained Plasmas in Flowing Argon," AIAA Journal, Vol. 24, No. 10, pp. 1656-1662, October 1986.

18. Glumb, R.J., and Krier, H., "A Two-Dimensional Model of Laser-Sustained Plasmas in Axisymmetric Flowfields," AIAA Journal, Vol. 24, No. 8, pp. 1331-1336, August 1986.

19. Zerkle, D.K., Schwartz, S., Mertogul, A.E., Chen, X., Krier, H., and Mazumder, J., "Laser-Sustained Argon Plasmas for Thermal Rocket Propulsion," AIAA Paper No. 88-2773, June 1988.

20. Bender, T.B., M.S. Thesis, Engineering Design, Fabrication, and Performance Evaluation of Laser Heated Gas Flow Facility : Application to Laser Propulsion, Department of Mechanical and Industrial Engineering, University of Illinois at Urbana-Champaign, 1985.

21. McMillin, B. K., Energy Conversion in Laser Sustained Argon Plasmas for Application to Rocket Propulsion, M.S. Thesis, Department of Mechanical and Industrial Engineering, University of Illinois at Urbana-Champaign, August, 1987.

22. Zerkle, D.K., Energy Conversion Measurements in Laser-Sustained Argon Plasmas at Elevated Mass Flux And Pressure, M.S. Thesis, Department of Mechanical and Industrial Engineering, University of Illinois at Urbana-Champaign, May 1988.

23. Chen, X., Spectroscopic Diagnostics of Argon Plasmas During Laser-Gas Interaction, M.S. Thesis, Department of Mechanical and Industrial Engineering, University of Illinois at Urbana-Champaign, August, 1988.

24. Mertogul, A.E., Energy Absorption and Thermal Conversion Efficiency in Argon Laser Sustained Plasmas, M.S. Thesis, Department of Aeronautical and Astronautical Engineering, University of Illinois at Urbana-Champaign, January, 1989.

25. Dresvin, S.V., Physics and Technology of Low Temperature Plasmas, Iowa State University Press, Ames, Iowa, 1977.

26 Drellishak, K.S., Knopp, C.F., and Cambel, A.B., "Partition Functions and Thermodynamic Properties of Argon Plasma," Arnold Engineering Development Center, Tennessee. AEDC-TDR-63-146.

27. Griem, H.R., Plasma Spectroscopy, McGraw-Hill Book Company, 1964.

28. Eddy, T.L., "Electron Temperature Determination ir LTE and non-LTE Plasmas," Journal of Quantitative Spectroscopic Radiative Transfer, Vol. 33, No. 3, pp. 197-211, 1985.

29. Griem, H.R., Spectral Line Broadening by Plasmas, Academic Press, 1974.

30. Smith, J.R., "Rayleigh Temperature Profiles in a Hydrogen Diffusion Flame," Rayleigh Spectroscopy, Vol. 158, pp. 84-90, 1978.

31. Two-Six Incorporated, "Technical Data Sheet," Form No. 7, Revision A, Two-Six Incorporated, Saxonburg, Pennsylvania, 1987.

32. Schwartz, S. "Energy Conversion Experiments with Laser-Sustained Argon Plasmas: Results and Operating System Update," ME 393 Final Report, Department of Mechanical and Industrial Engineering, University of Illinois at Urbana-Champaign, December 1987.

33 . Holman, J.P., Experimental Methods for Engineers, Fourth Edition, McGraw-Hill Book Company, 1984.

34. Cherrington, B.E., Gaseous Electronics and Gas Lasers, Pergamon Press, 1979.

35. Jeng, S-M., and Keefer, D.R., "Theoretical Investigation of Laser-Sustained Argon Plasmas", Journal of Applied Physics, Vol. 60(7), pp.2272-2279, October 1, 1986.

36. Patankar, S.V., Numerical Heat Transfer and Fluid Flow, Hemisphere Publishing Corporation, New York, 1980.

37. Personal communication with Dr. San-Mou Jeng at the University of Tennessee Space Institute on December 12, 1988.

38. Howell, J.R., and Buckius, R.O., Fundamentals of Engineering Thermodynamics, McGraw-Hill Book Company, New York, 1987.

39. Vargaftik, N.B., Tables on the Thermophysical Properties of Liquids and Gases, Hemisphere Publishing Corporation, 1975.

40. Sergienko, A.S., and Fokov, G.A., "Calculation of the Characteristics of a Direct Current Argon Arc", Journal of Engineering Physics, Vol. 32, April 1977, pp.399-403.

41. Bues, J., Z. Angew. Phys., Vol. 22, pp.345, 1967.

42. DeVoto, R.S., "Transport Coefficients of Ionized Argon", The Physics of Fluids, Vol. 16, No. 1, pp.616-623, 1972.